Supplementary Information for

A simple, sustainable route to flexible microporous carbon cloth for energy storage applications

Thria Alkhaldi [a, b], L. Scott Blankenship [a], and Robert Mokaya [a]

* *E-Mail: r.mokaya@nottingham.ac.uk*

[a]School of Chemistry, University of Nottingham, University Park, Nottingham, NG7 2RD, UK.
[b]Department of Chemistry, Jeddah University, Jeddah 23442, Saudi Arabia

1. Synthesis

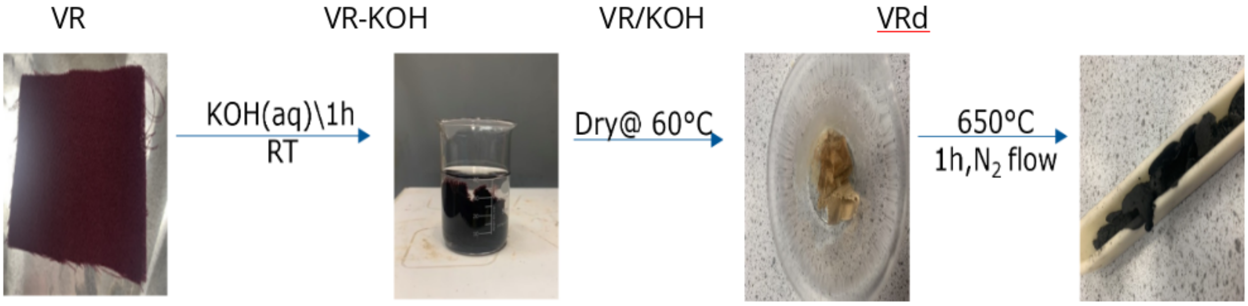

Fig. S1: Steps in the direct activation of viscose rayon (VR) with KOH. This process yields powdered activated carbon.

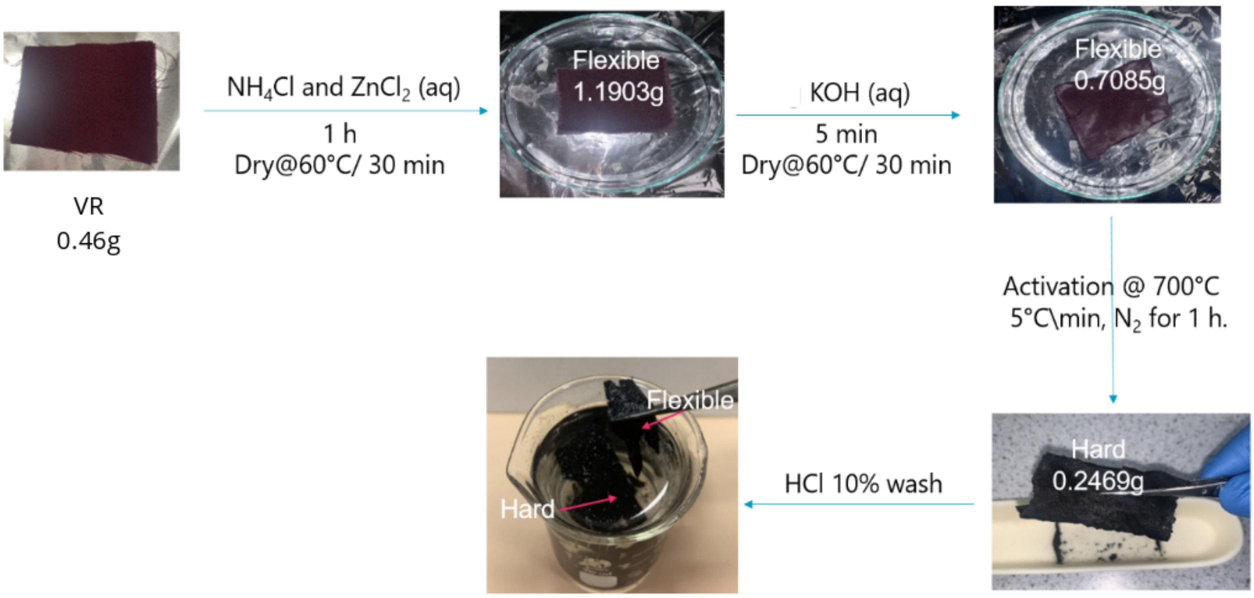

Fig. S2: Steps in the stabilisation of viscose rayon (VR) with NH_4Cl and $ZnCl_2$ prior to activation with KOH. This process yields both hard (powdered) and flexible activated carbon.

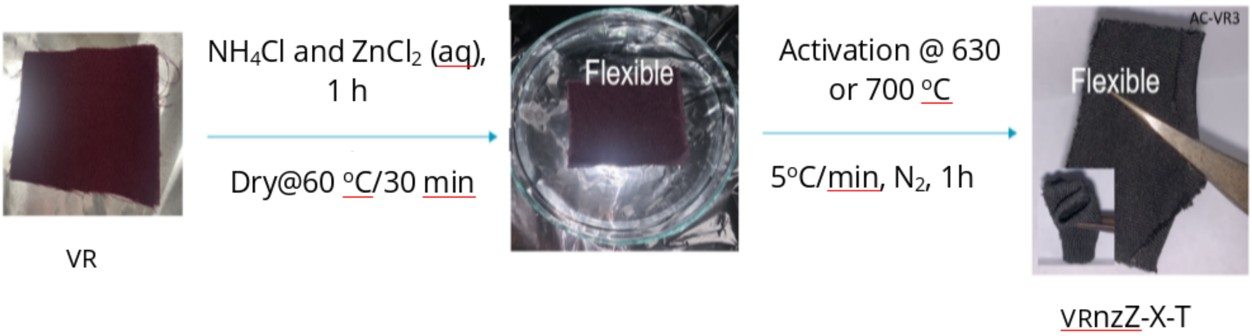

Fig. S3: Steps in the stabilisation of viscose rayon (VR) with NH_4Cl and $ZnCl_2$ prior to thermal treatment to facilitate activation with the latter ($ZnCl_2$). This process yields flexible activated carbon cloth - series VRnzZ-*X*-*T*.

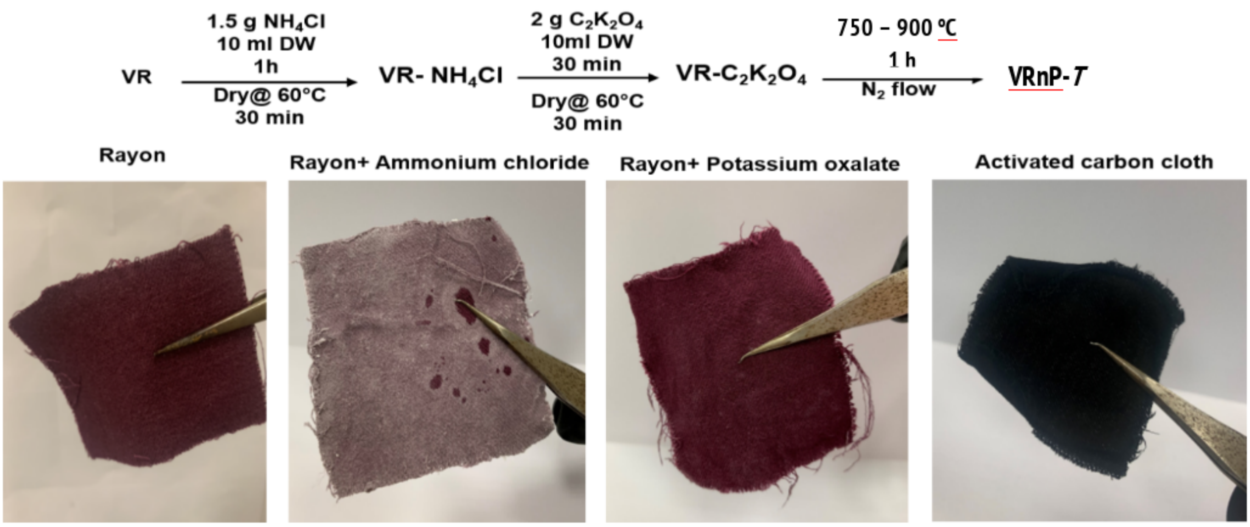

Fig. S4: Steps in the stabilisation of viscose rayon (VR) with NH_4Cl only followed by activation with PO. This process yields flexible activated carbon cloth - series VRnP-*T*.

2. Powder X-ray Diffraction

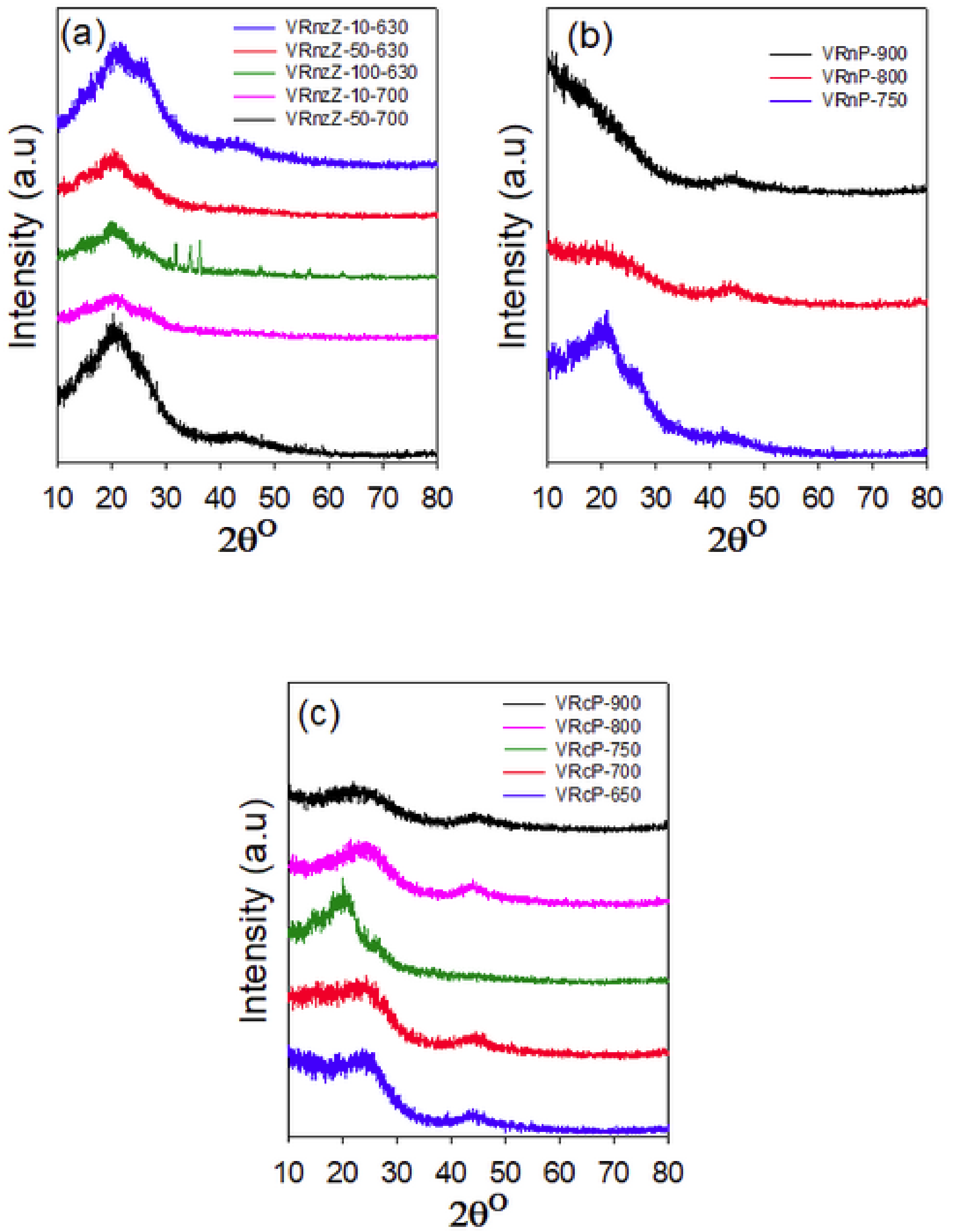

Fig. S5: XRD patterns of flexible VR-derived ACCs; (a) series VRnzZ-*X*-*T*, (b) series VRnP-*T*, and (c) series VRcP-*T*.

3. Thermogravimetric Analysis

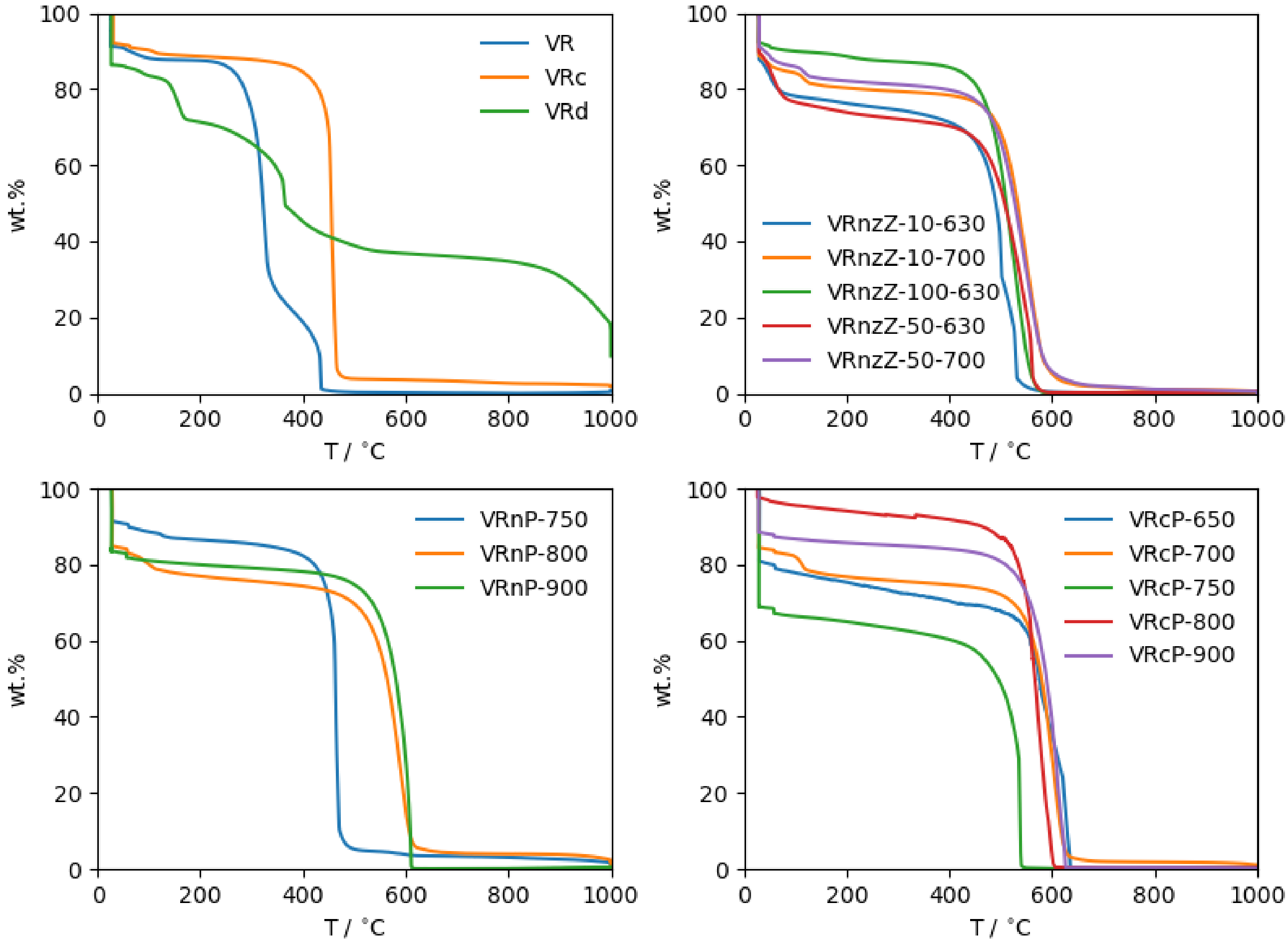

Fig. S6: TGA curves of VR, powdered carbons and flexible ACCs synthesised in this work.

4. Scanning electron Microscopy

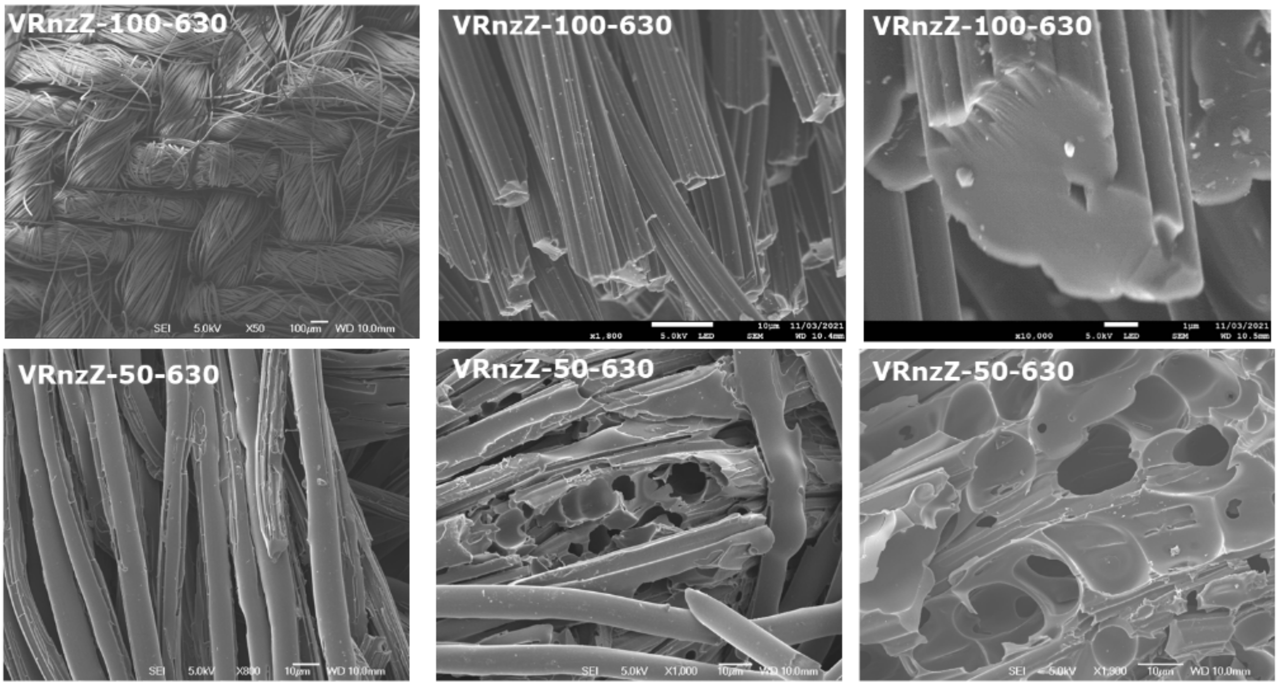

Fig. S7: SEM images of series VRnzZ-X-T flexible VR-derived ACCs activated at 630 °C.

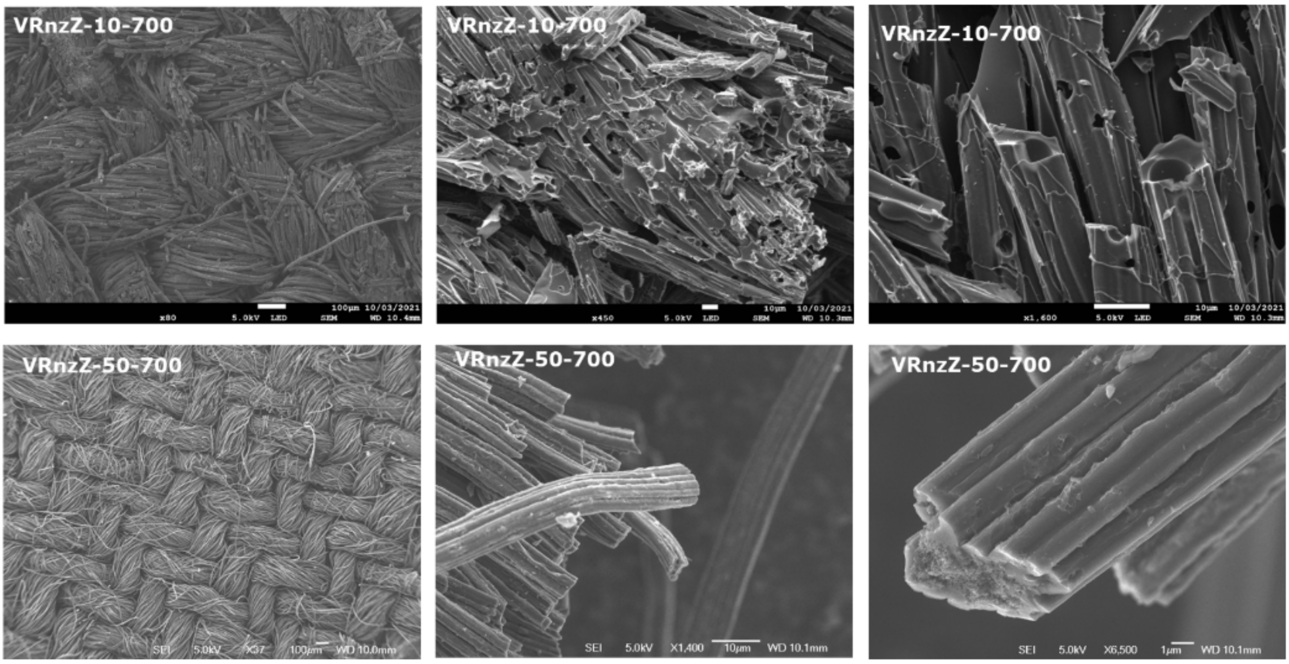

Fig. S8: SEM images of series VRnzZ-X-T flexible VR-derived ACCs activated at 700 °C.

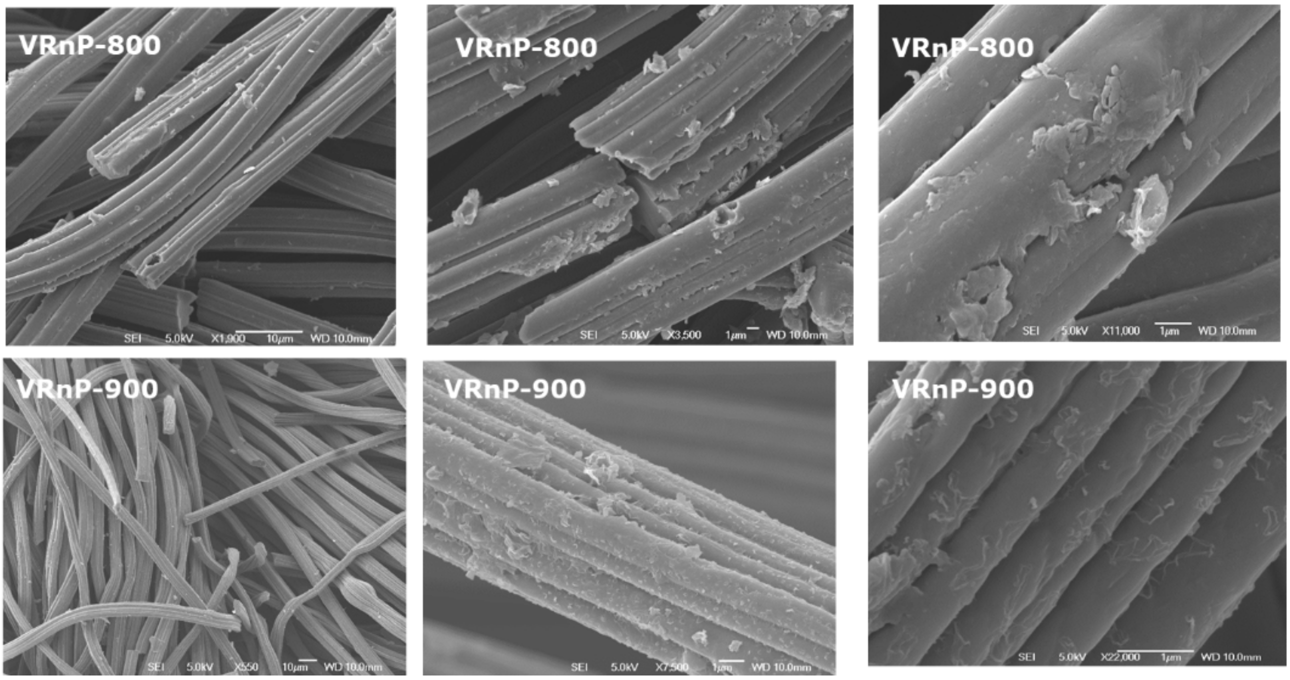

Fig. S9: SEM images of VRnP-*T* flexible VR-derived ACCs.

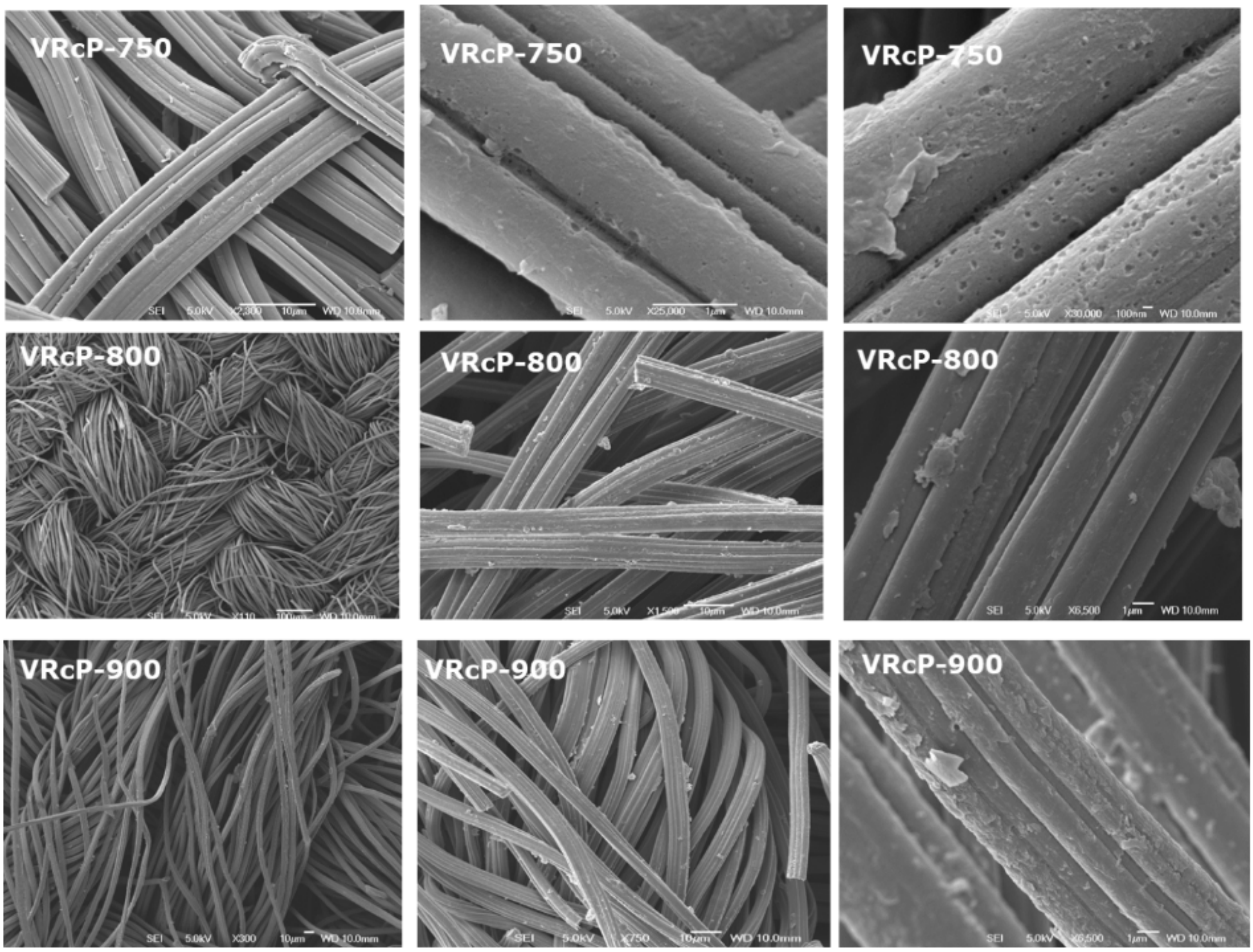

Fig. S10: SEM images of series VRcP-T flexible VR-derived ACCs

5. Isotherm measurement conditions

Table S1: Conditions used for measurin N_2 isotherms for porosimetry. Pressure points either controlled by initial and final relative pressure, a relative pressure increment or quantity of gas dosed. Equilibration time (t_E) was higher at low pressures due to equilibration issues in small pores.[S1]

P/P_0 initial	P/P_0 increment	dose / $cm^3\ g^{-1}{}_{stp}$	t_E/ s	P/P_0 final
0.00e+00		10	45	4.00e-04
4.00e-04		25	35	1.00e-01
1.00e-01	0.05		10	1.50e-01
1.50e-01	0.05		10	2.00e-01
2.00e-01	0.05		10	2.50e-01
2.50e-01	0.05		10	3.00e-01
3.00e-01	0.05		10	3.50e-01
3.50e-01	0.05		10	4.00e-01
4.00e-01	0.05		10	4.50e-01
4.50e-01	0.05		10	5.00e-01
5.00e-01	0.05		10	5.50e-01
5.50e-01	0.05		10	6.00e-01
6.00e-01	0.05		10	6.50e-01
6.50e-01	0.05		10	7.00e-01
7.00e-01	0.05		10	7.50e-01
7.50e-01	0.05		10	8.00e-01
8.00e-01	0.05		10	8.50e-01
8.50e-01	0.05		10	9.00e-01
9.00e-01	0.05		10	9.50e-01
9.50e-01			10	9.90e-01
9.90e-01			10	9.95e-01
9.95e-01			10	9.98e-01
9.98e-01			10	9.95e-01
9.95e-01			10	9.90e-01
9.90e-01			10	9.50e-01
9.50e-01			10	9.00e-01
9.00e-01			10	8.50e-01
8.50e-01			10	8.00e-01
8.00e-01			10	7.50e-01
7.50e-01			10	7.00e-01
7.00e-01			10	6.50e-01
6.50e-01			10	6.00e-01
6.00e-01			10	5.50e-01
5.50e-01			10	5.00e-01
5.00e-01			10	4.50e-01
4.50e-01			10	4.00e-01
4.00e-01			10	3.50e-01
3.50e-01			10	3.00e-01
3.00e-01			10	2.50e-01
2.50e-01			10	2.00e-01
2.00e-01			10	1.50e-01
1.50e-01			10	1.00e-01

6. BETSI analysis

BETSI analysis[S2] was performed with the constraints of having maximum percentage error of 20 %, a minimum r^2 of 0.995, and starting with a minimum number of 10 points. In cases where a 10 point range could not be found to satisfy the other requirements, this number was reduced and the calculation repeated until a fit could be achieved - in this study this only applied to VRnzZ-10-700. Results summary is tabulated in table S2.

Table S2: Summary of BETSI results for optimum fitting. An r^2 of >0.9999 was consistently rounded down as opposed to rounding up to 1.0000 as to not give the false impression of a perfect fit.

Sample	$\mathbf{A_{BET}}$/ $m^2\,g^{-1}$	**points**	$\mathbf{r^2}$	**Slope**	**intercept**	C	$\mathbf{Q_m}$ / $cm^3\,g^{-1}{}_{stp}$
VRd	939	11	0.9996	0.004635	2.144×10^{-7}	21620	215.7
VRnzK-700 (hard)	1503	12	0.9999	0.002892	3.789×10^{-6}	764.2	345.3
VRnzK-700 (flexible)	1010	29	0.9999	0.004302	7.652×10^{-6}	563.1	232.1
VRnzZ-10-630	947	11	0.9999	0.004596	2.641×10^{-6}	1741	217.4
VRnzZ-50-630	1222	11	0.9999	0.003561	1.248×10^{-6}	2856	280.7
VRnzZ-100-630	926	21	0.9998	0.004700	6.125×10^{-8}	76740	212.8
VRnzZ-10-700	598	7	0.9999	0.007284	1.573×10^{-7}	46290	137.3
VRnzZ-50-700	965	11	0.9999	0.004509	1.025×10^{-6}	4399	221.7
VRnP-750	1934	11	0.9999	0.002250	1.346×10^{-6}	1673	444.2
VRnP-800	993	11	0.9999	0.004381	1.039×10^{-6}	4220	228.2
VRnP-900	1095	11	0.9999	0.003971	1.546×10^{-6}	2570	251.7
VRc	85	11	0.9996	0.05139	4.637×10^{-5}	1109	19.44
VRcP-650	942	11	0.9996	0.004619	2.584×10^{-7}	17870	216.5
VRcP-700	1013	11	0.9996	0.004298	3.553×10^{-7}	12100	232.6
VRcP-750	2227	11	0.9996	0.001953	1.740×10^{-6}	1123	511
VRcP-800	713	11	0.9999	0.006107	2.005×10^{-6}	3048	163.7
VRcP-900	701	11	0.9999	0.006209	1.478×10^{-6}	4202	701.1

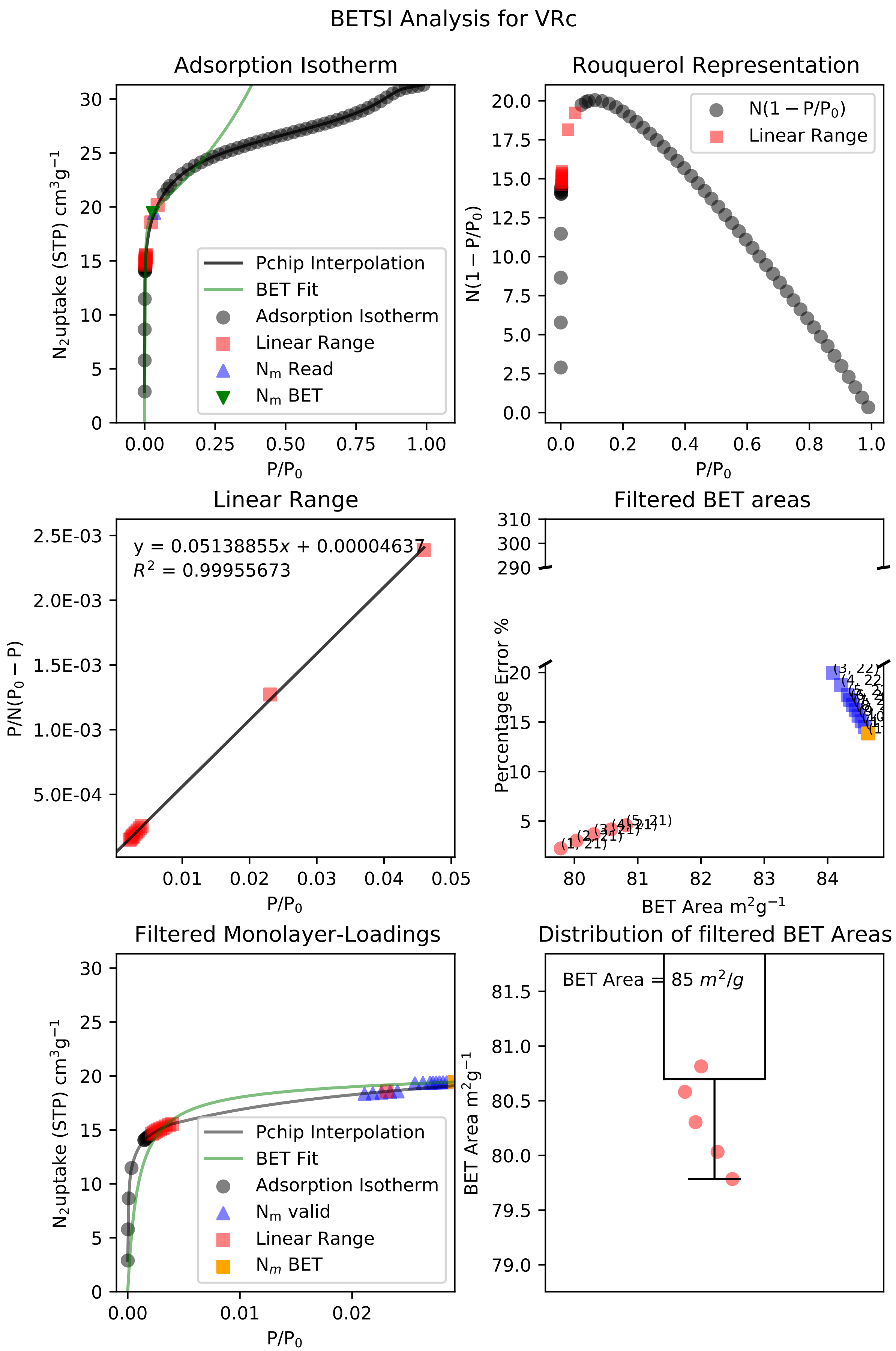

Fig. S11: BETSI analsysis for VRc.

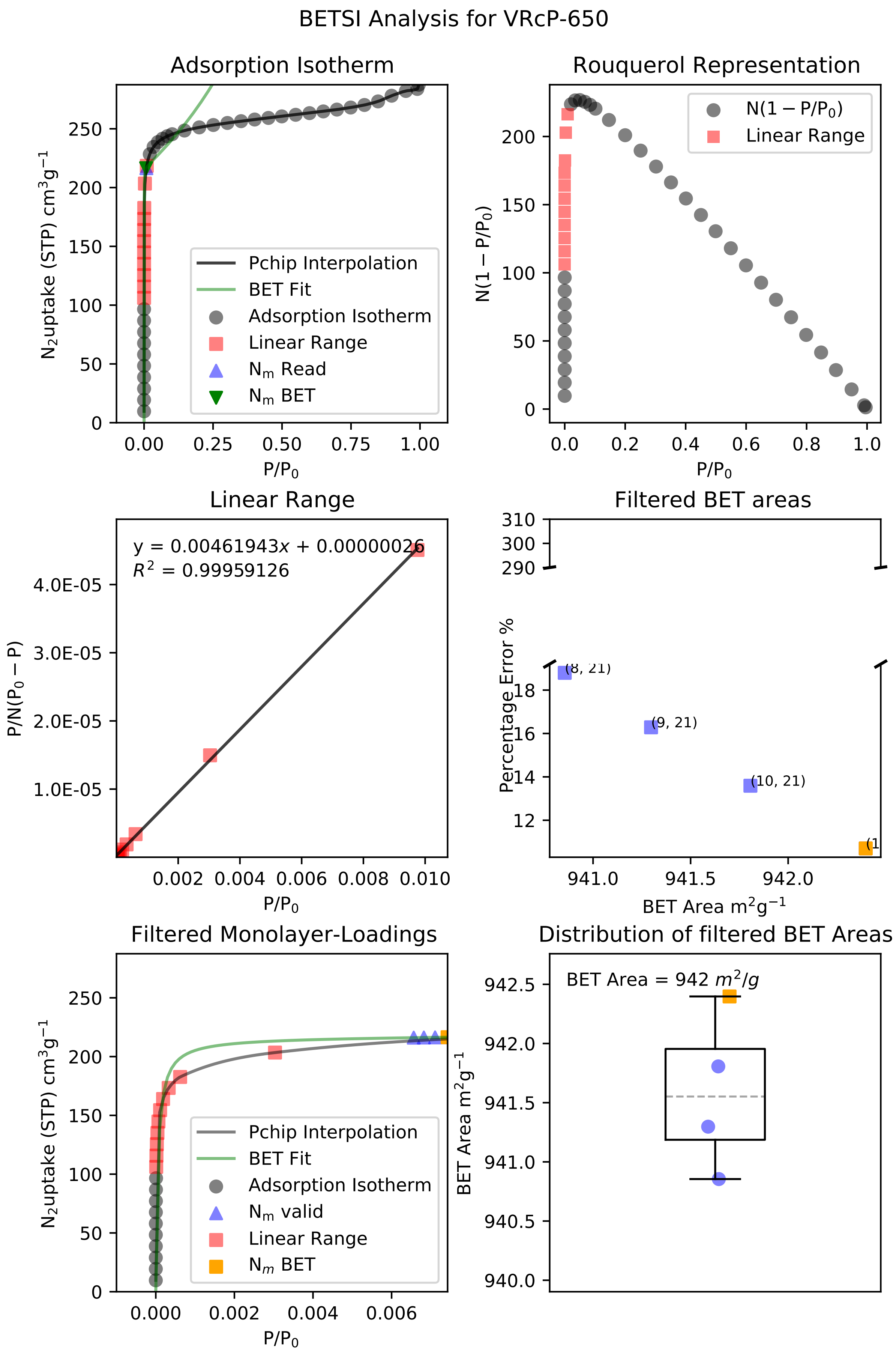

Fig. S12: BETSI analsysis for VRcP-650.

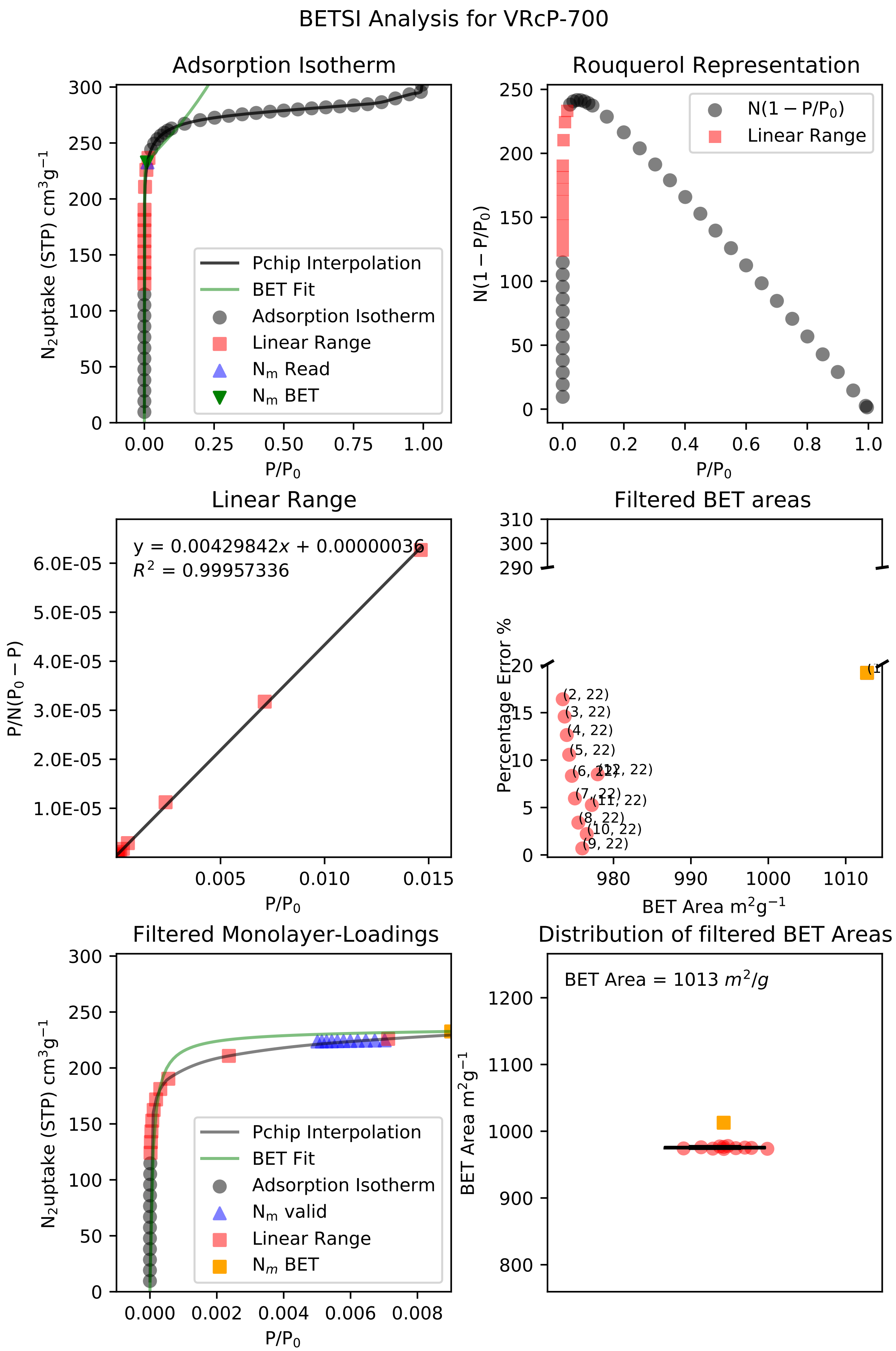

Fig. S13: BETSI analsysis for VRcP-700.

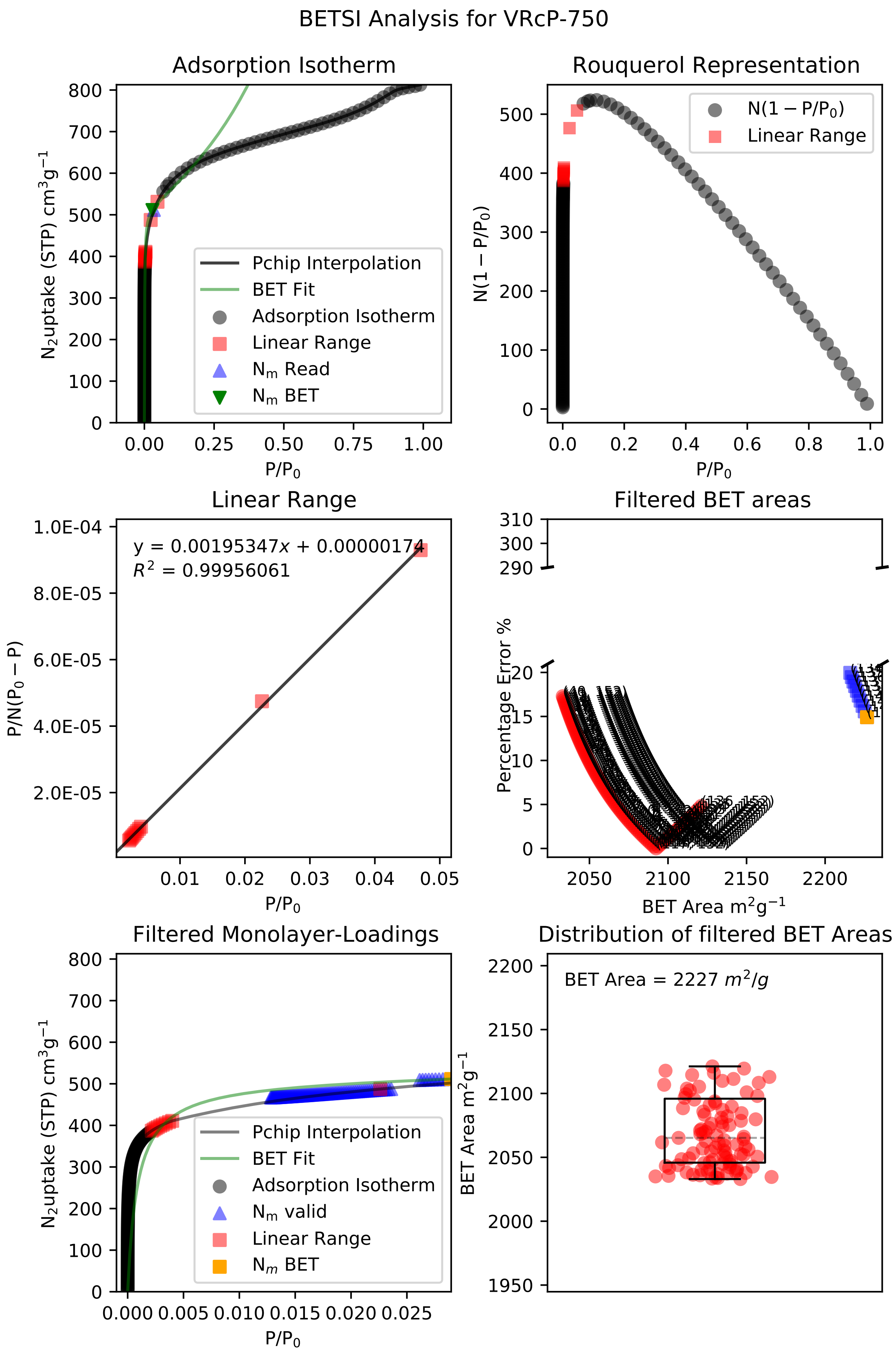

Fig. S14: BETSI analsysis for VRcP-750.

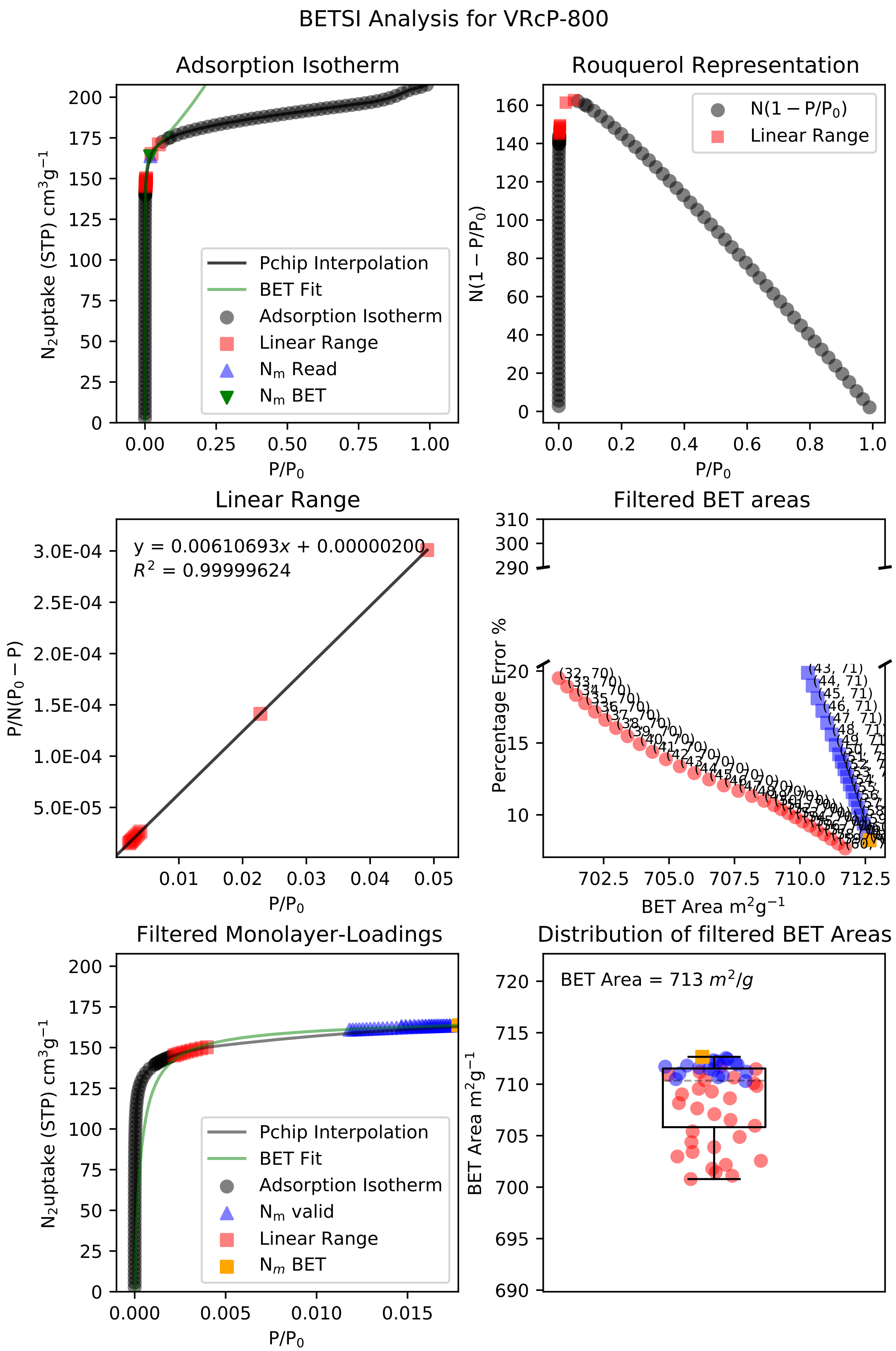

Fig. S15: BETSI analsysis for VRcP-800.

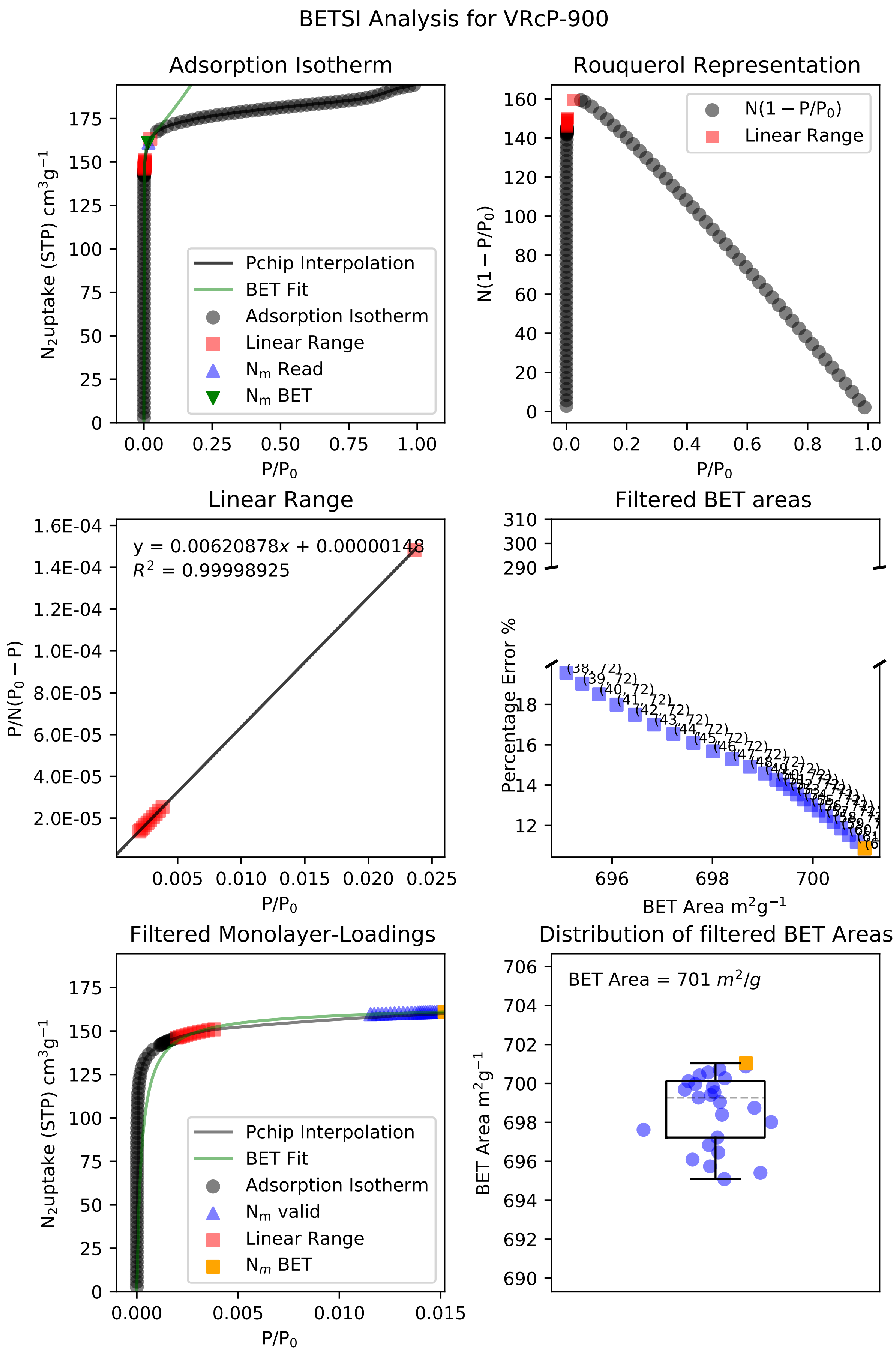

Fig. S16: BETSI analsysis for VRcP-900.

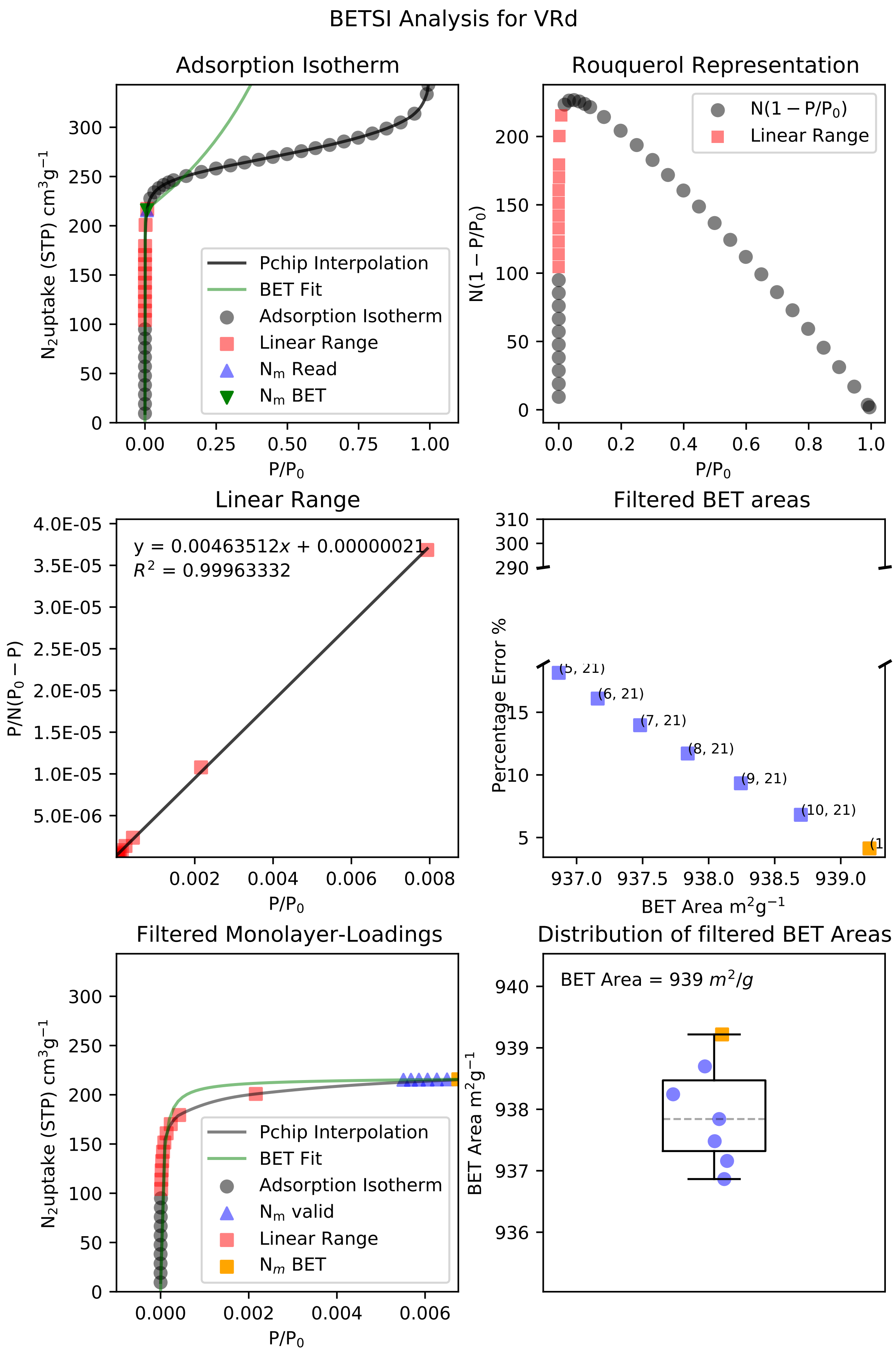

Fig. S17: BETSI analsysis for VRd.

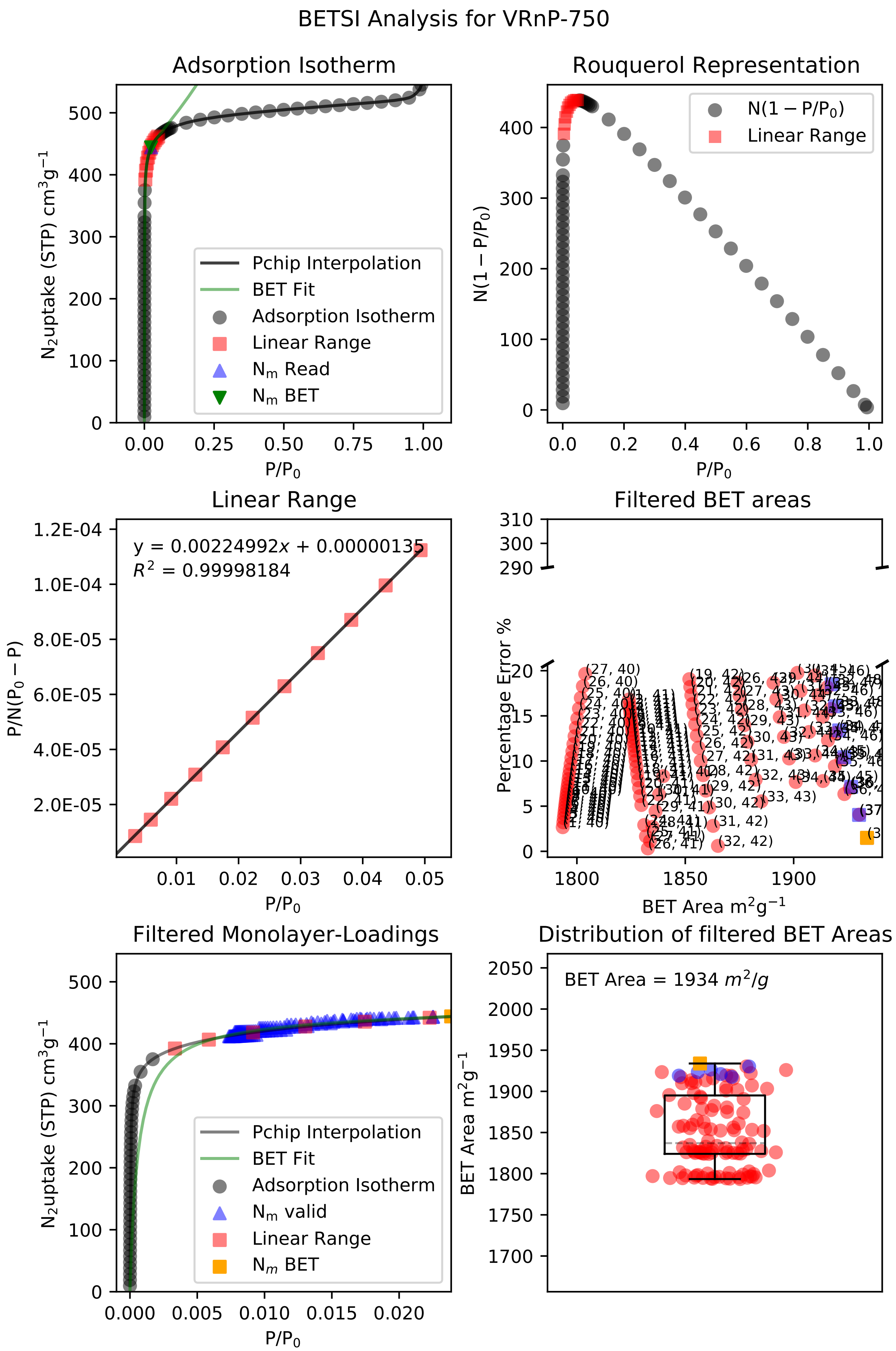

Fig. S18: BETSI analsysis for VRnp-750.

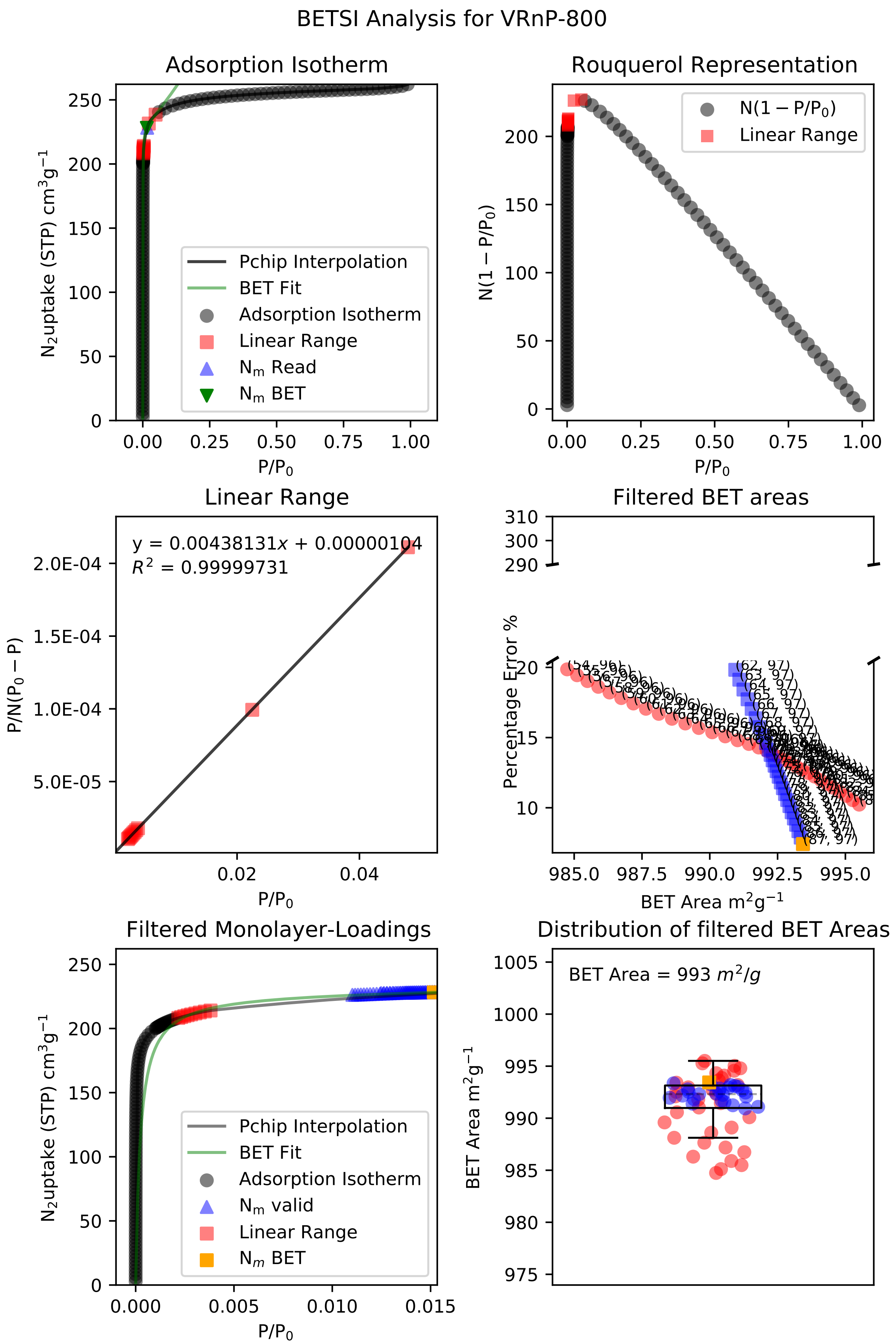

Fig. S19: BETSI analsysis for VRnP-800.

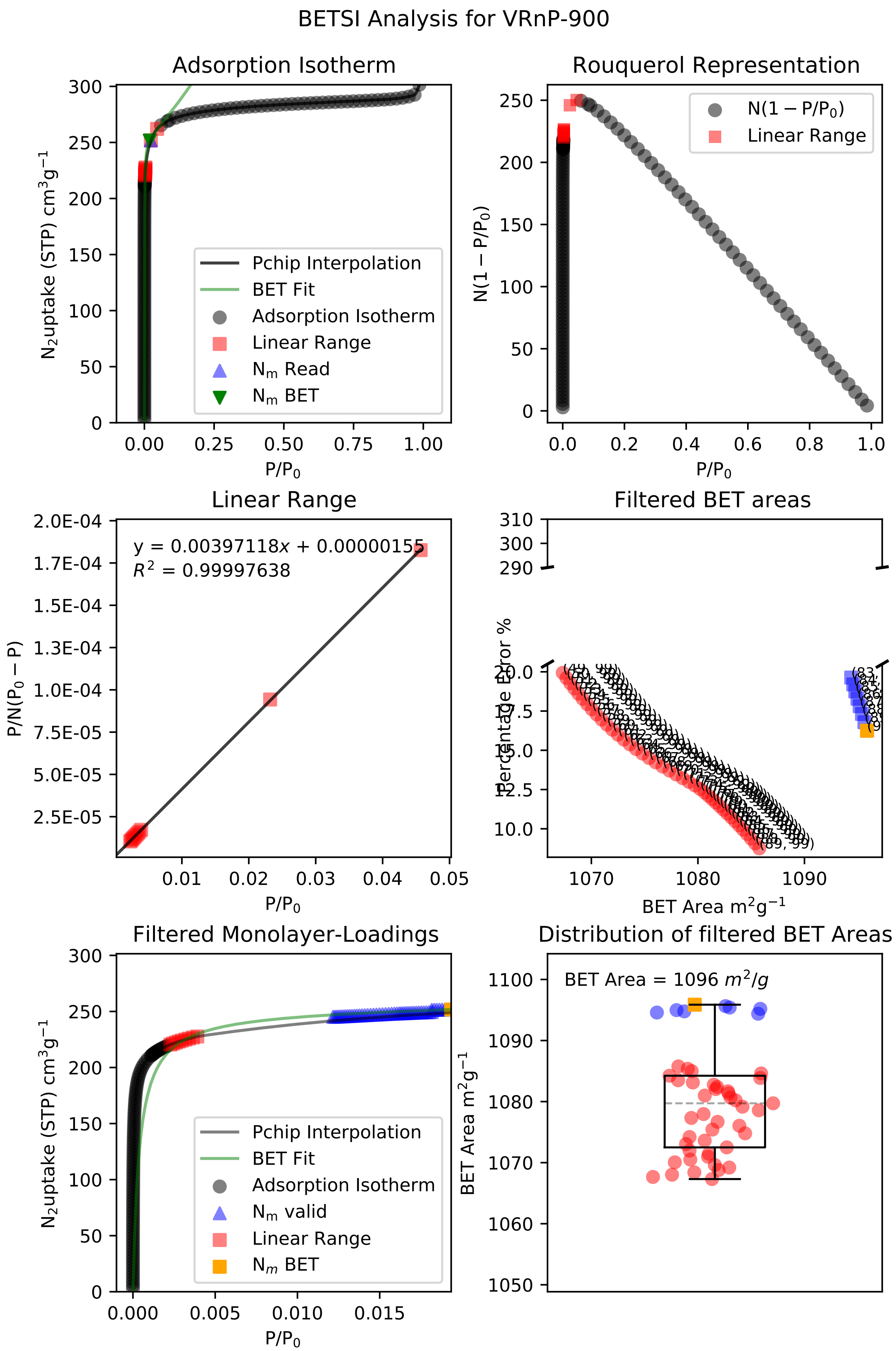

Fig. S20: BETSI analsysis for VRnP-900.

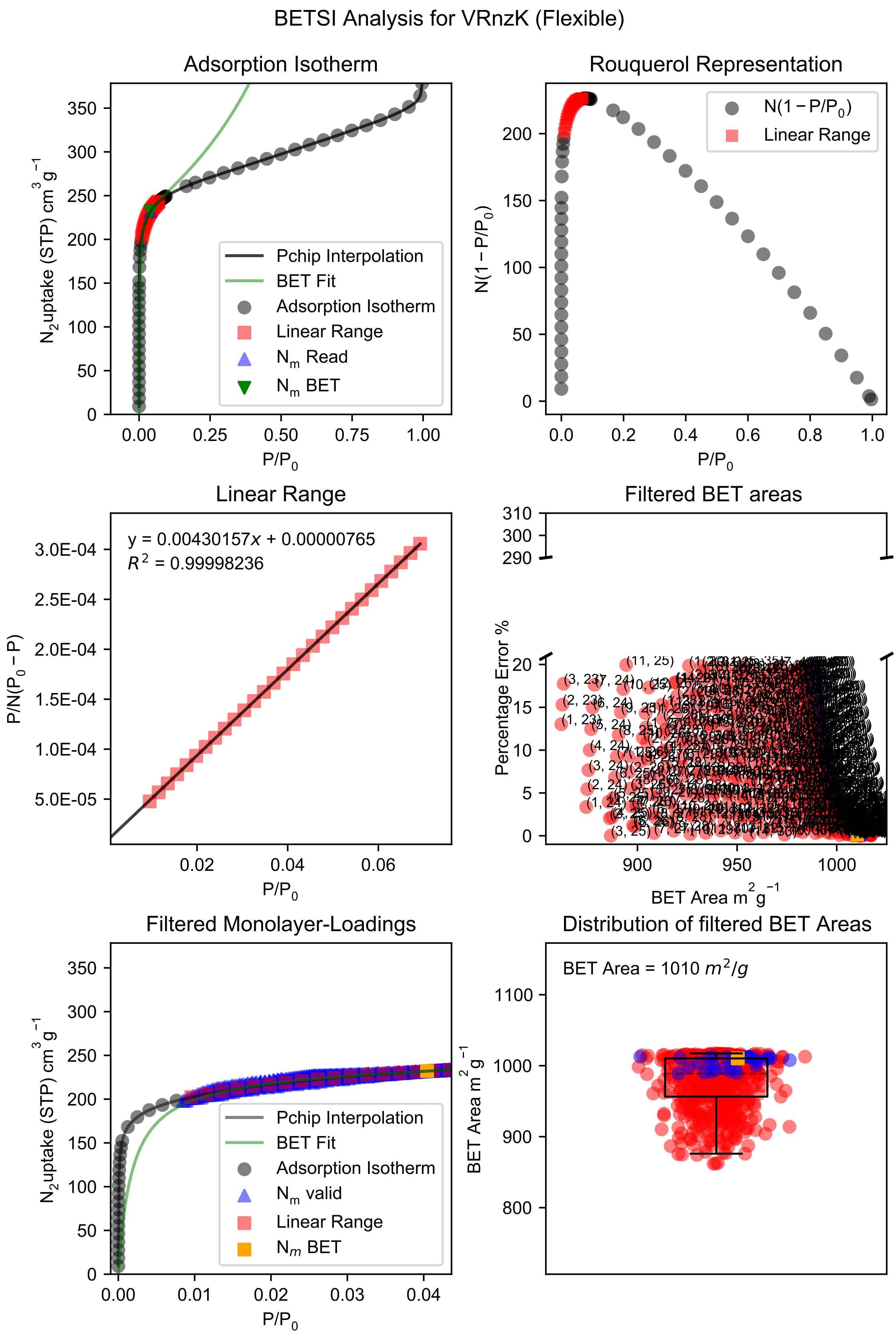

Fig. S21: BETSI analsysis for VRnzK (flexible).

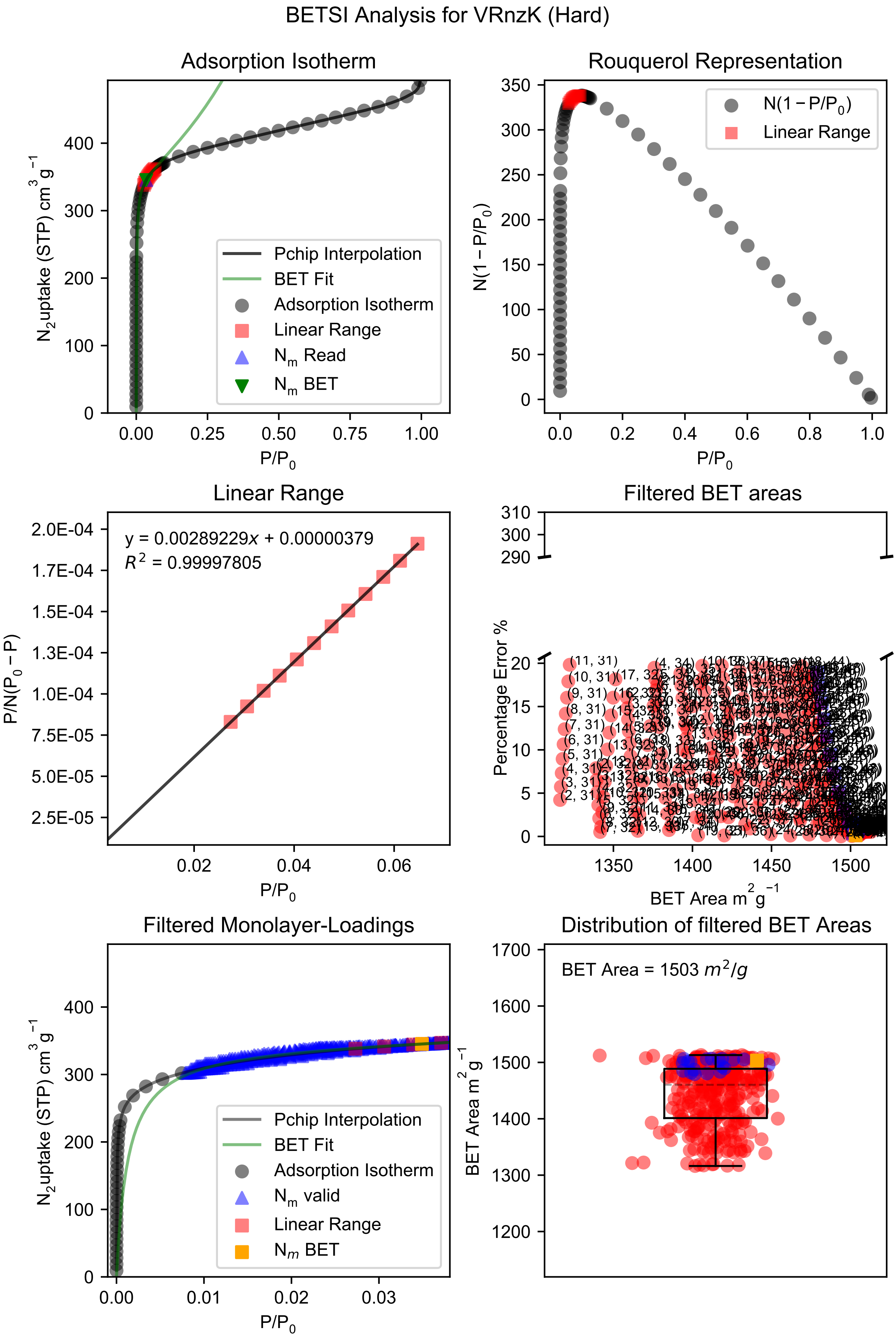

Fig. S22: BETSI analsysis for VRnzK (hard).

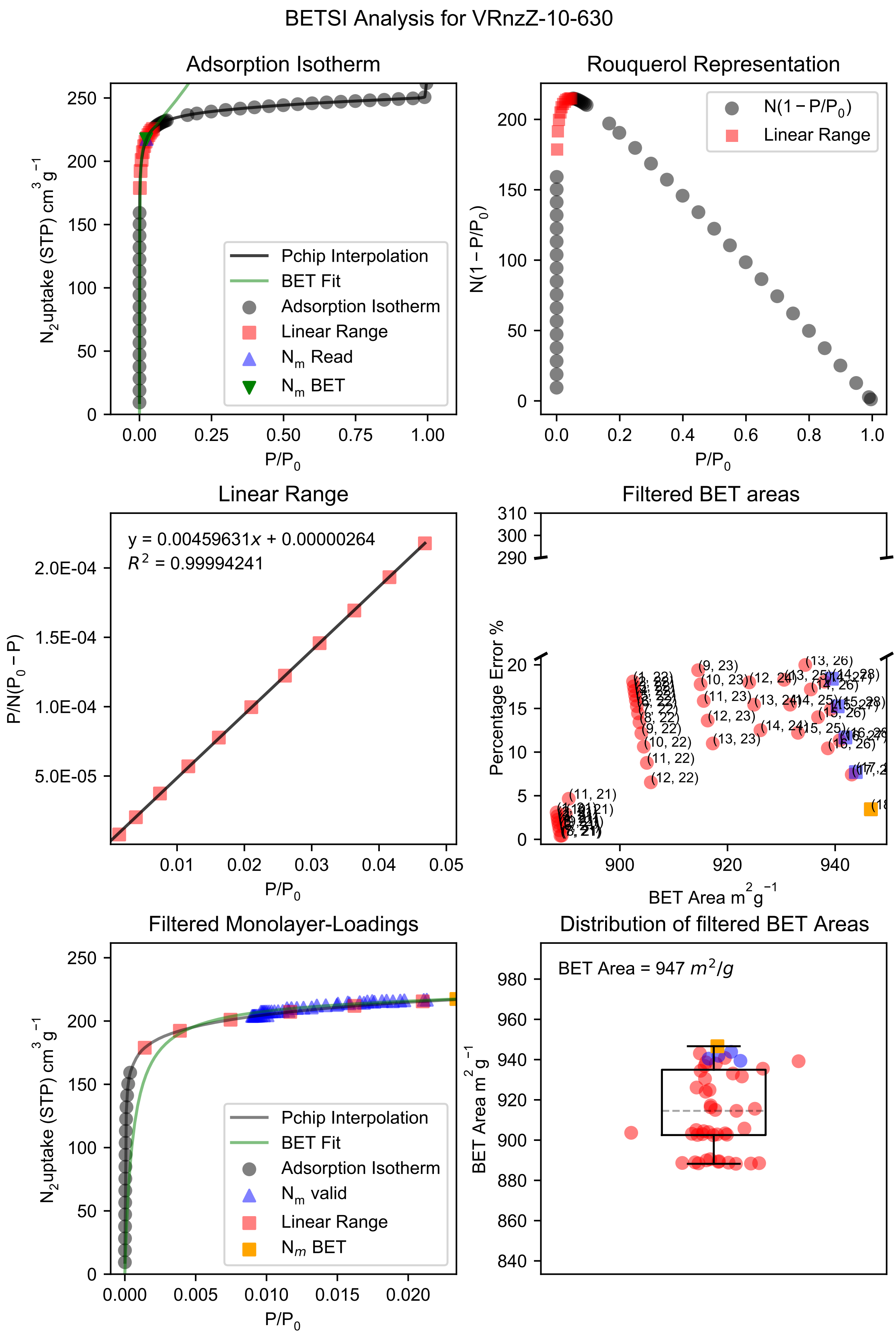

Fig. S23: BETSI analsysis for VRnzZ-10-630.

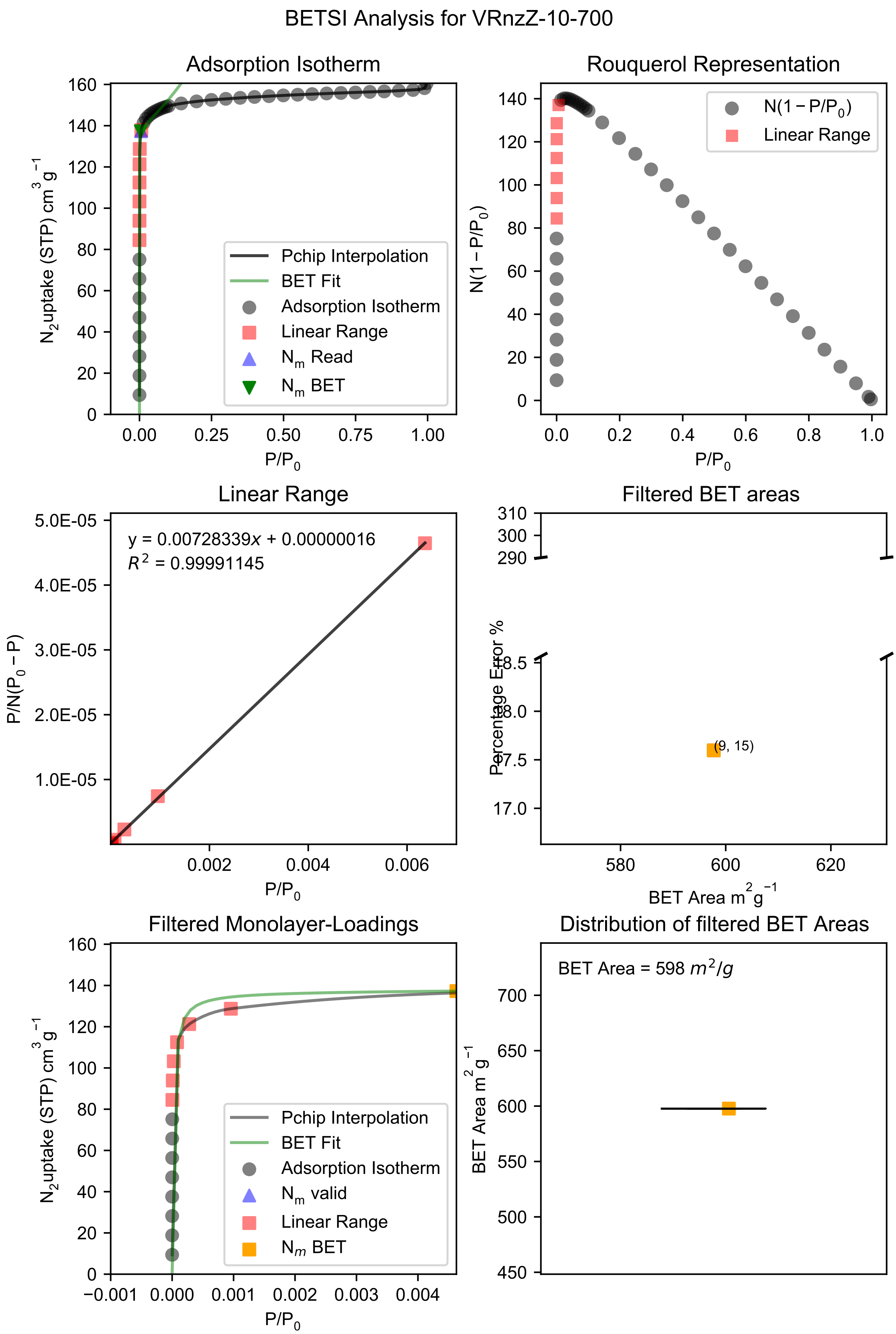

Fig. S24: BETSI analsysis for VRnzZ-10-700.

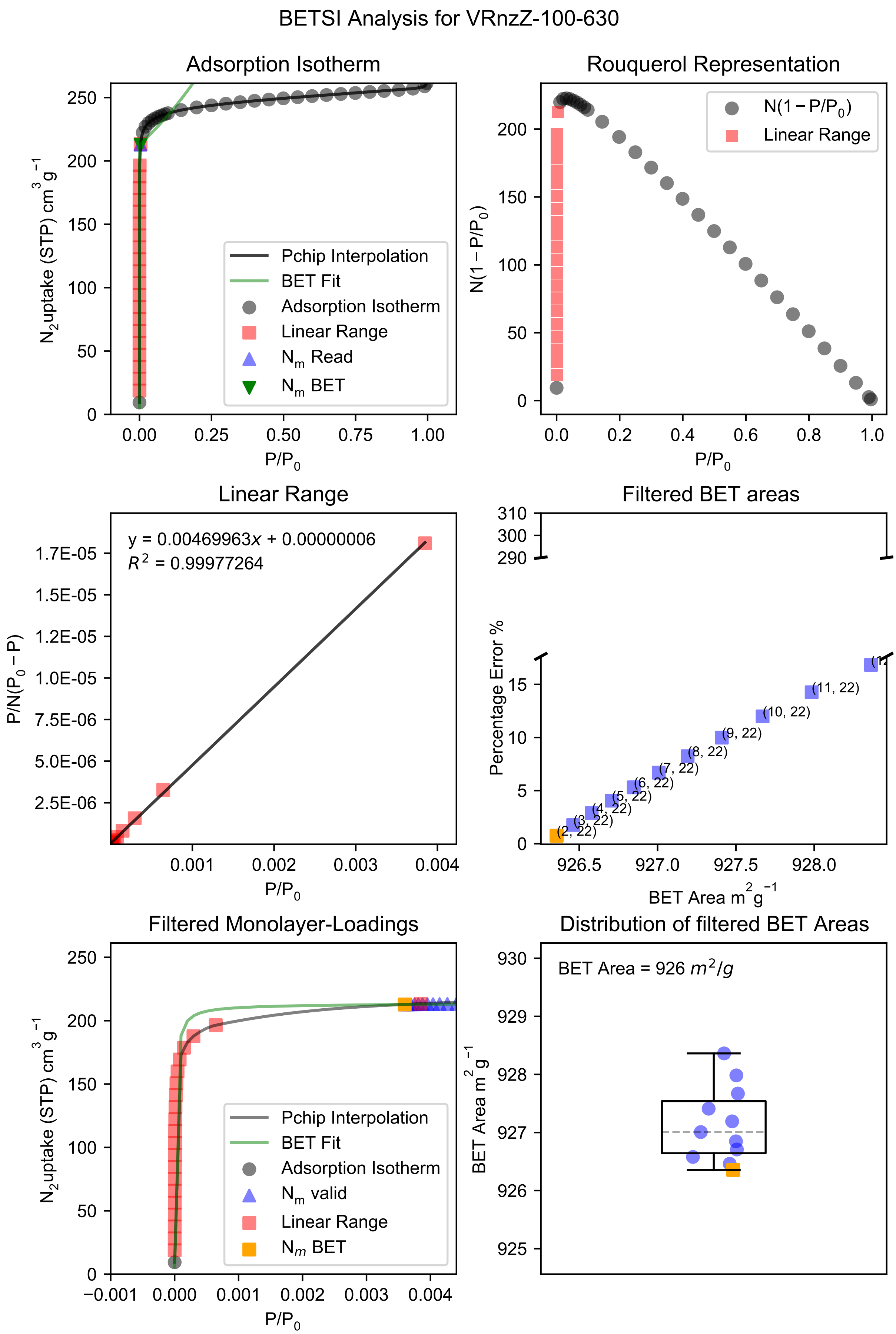

Fig. S25: BETSI analsysis for VRnzZ-100-630.

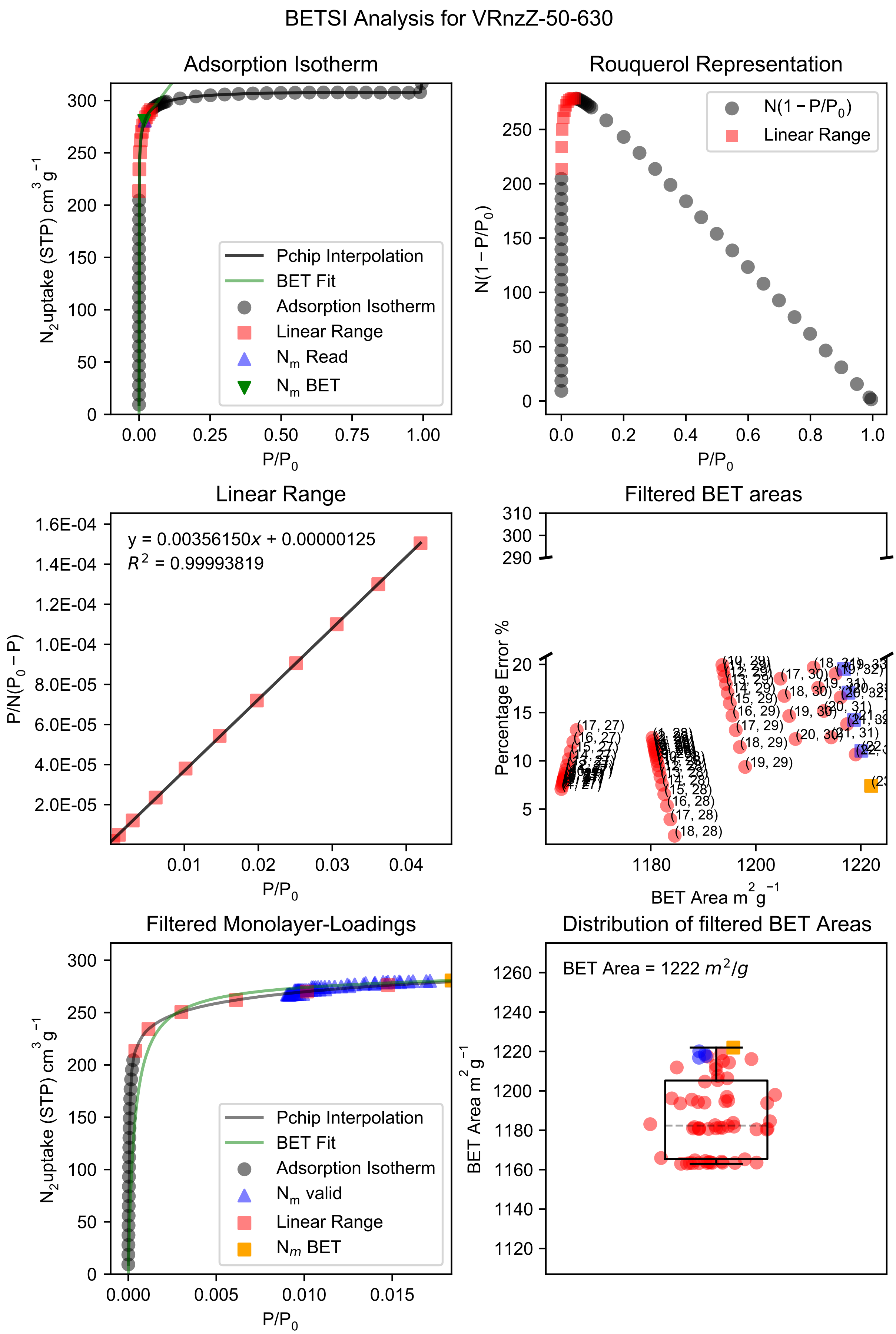

Fig. S26: BETSI analsysis for VRnzZ-50-630.

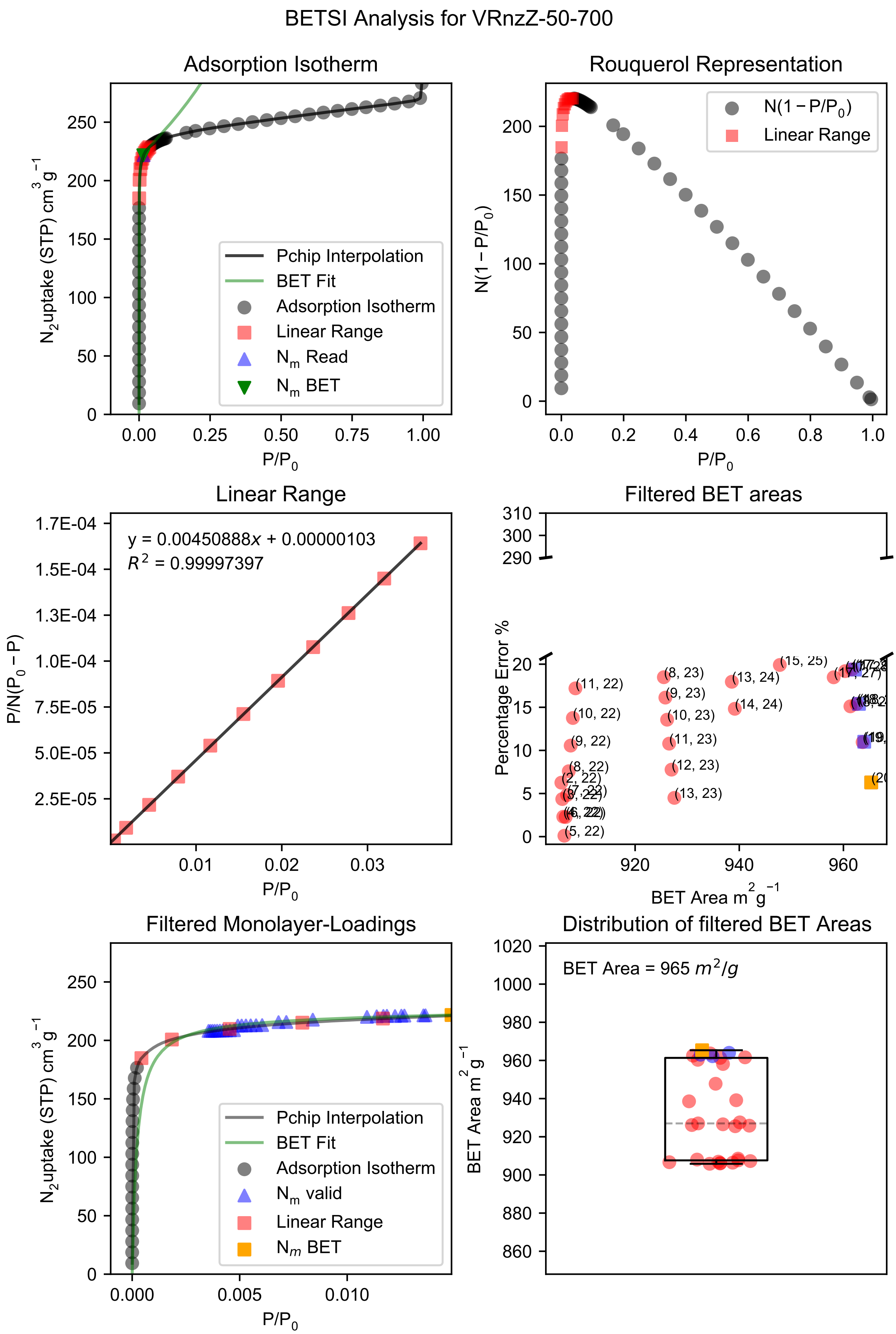

Fig. S27: BETSI analsysis for VRnzZ-50-700.

7. PSD determination

PSDs and fits of isotherms to 2D-NLDFT heterogenous surface kernel[S3] are included on the following pages.

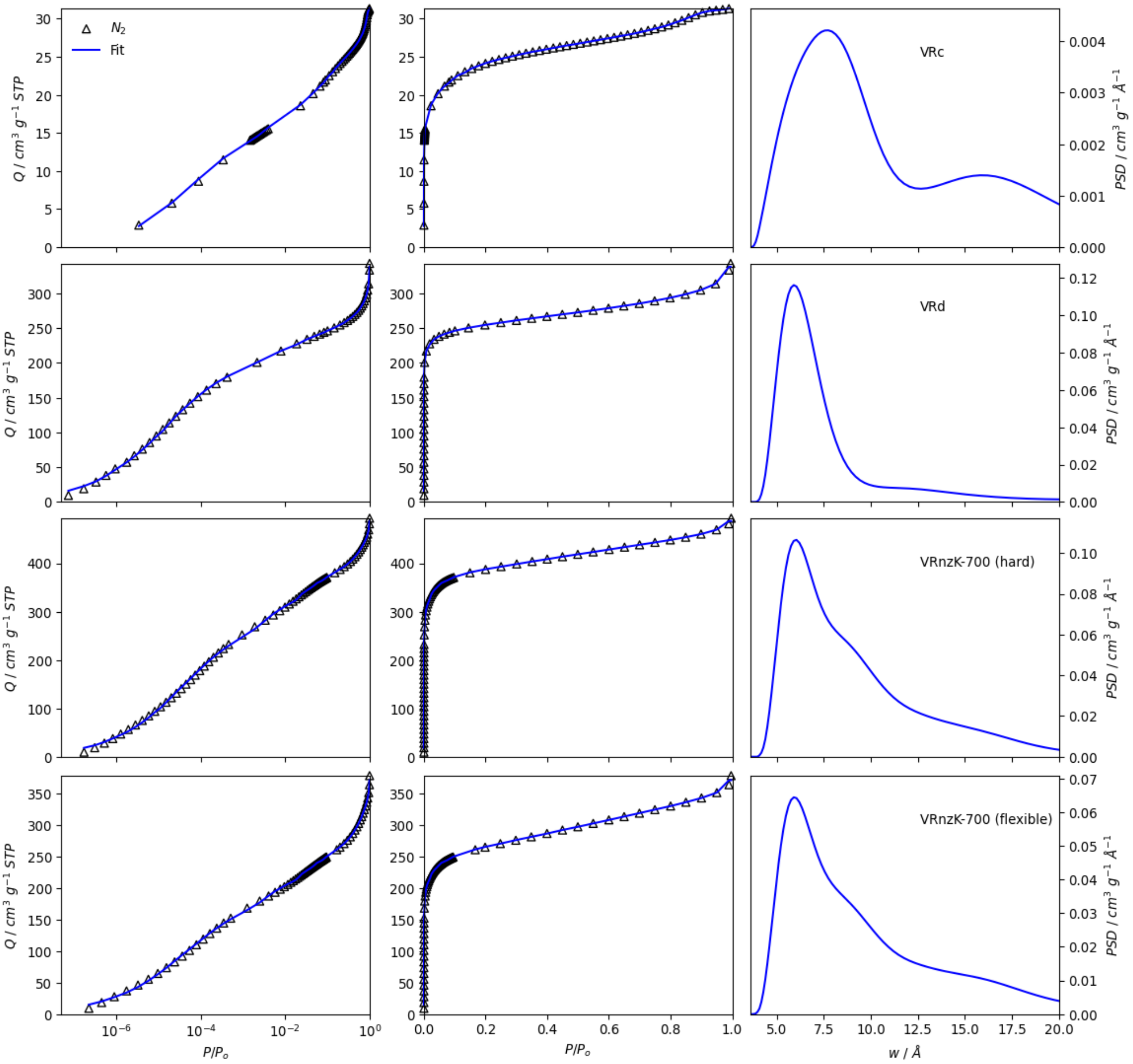

Fig. S28: Fits of N_2 isotherms of samples VRc, VRd, as well as hard and flexible portions of VRnzK-700.

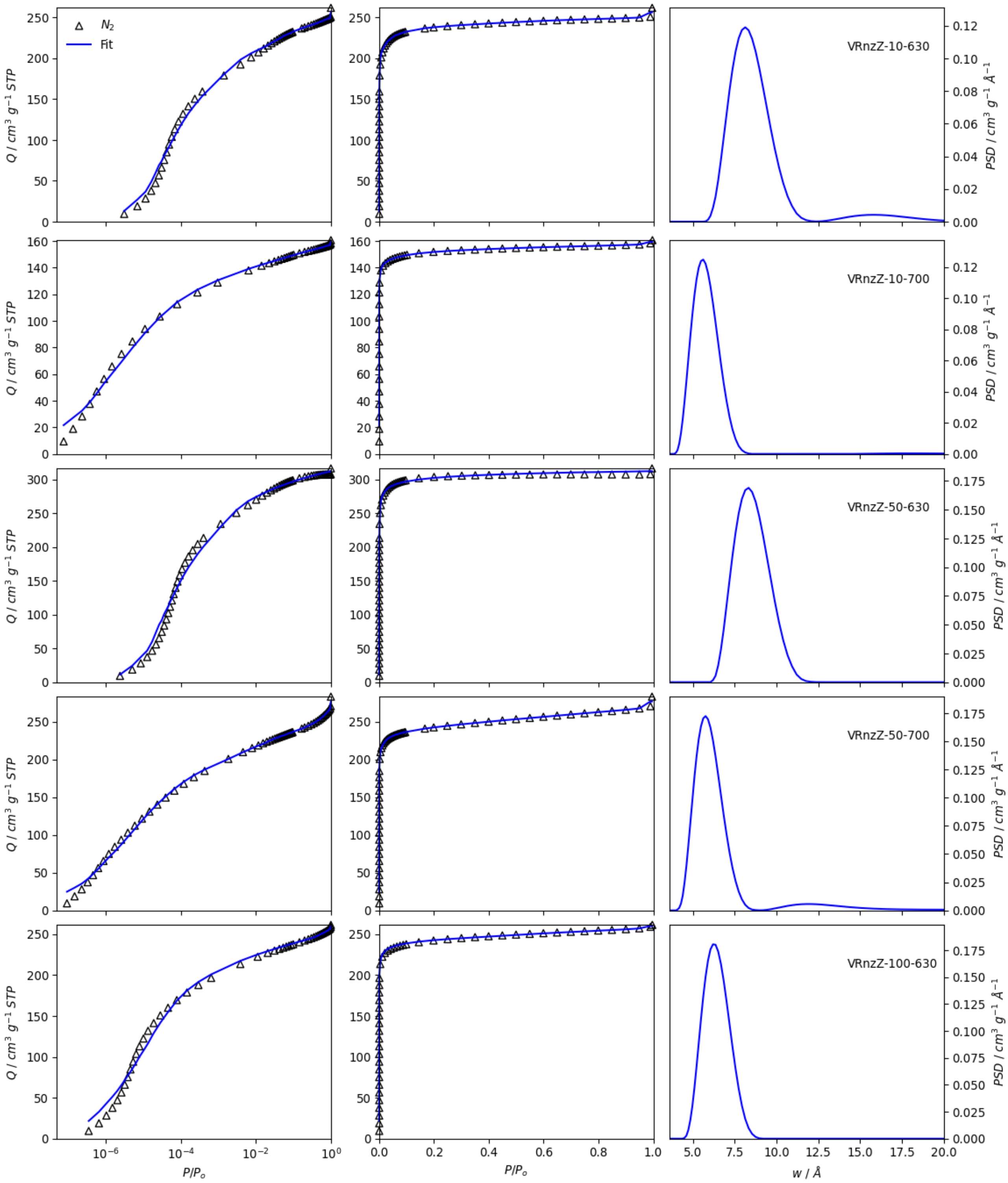

Fig. S29: Fits of N_2 isotherms of samples in set VRnzZ-*X*-*T*.

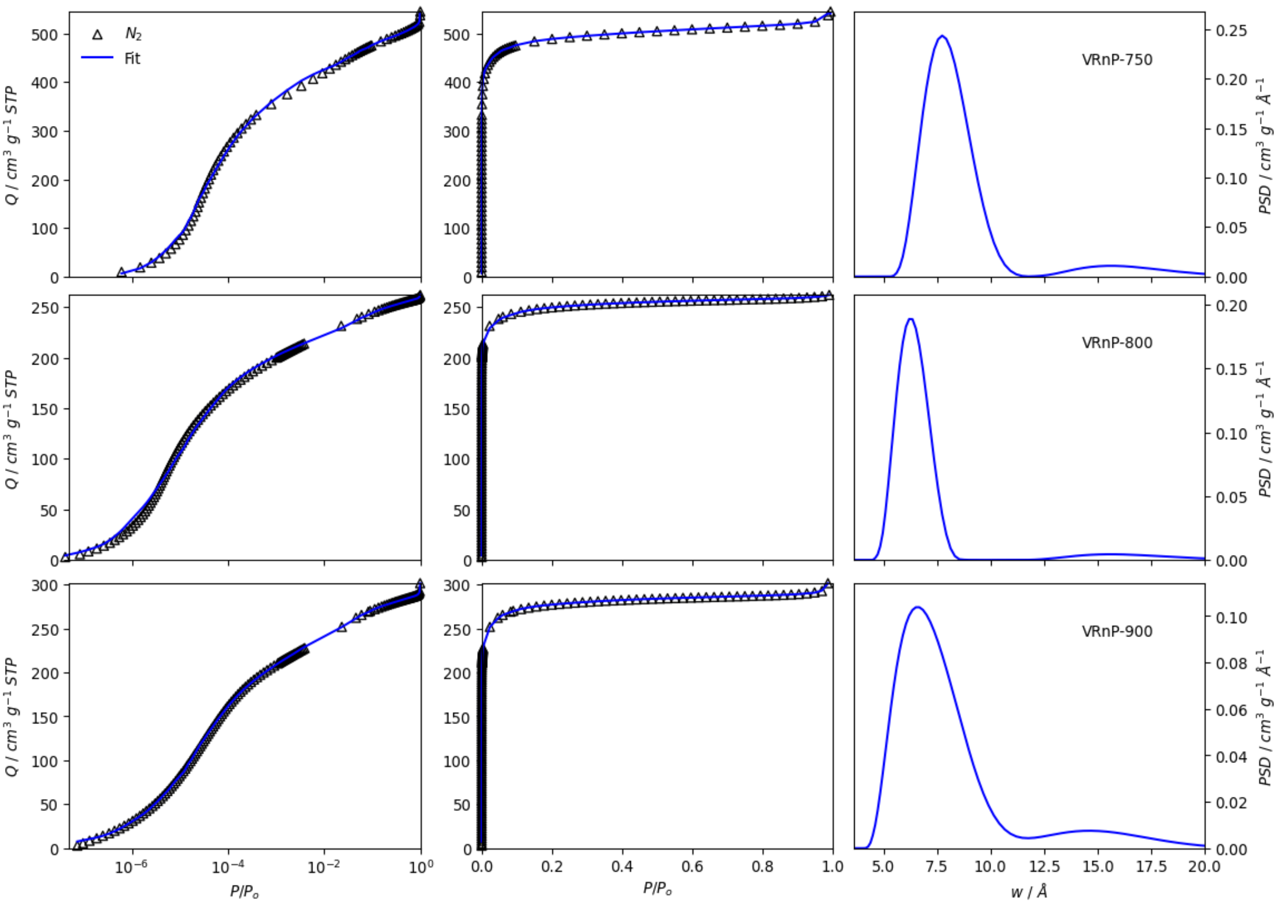

Fig. S30: Fits of N_2 isotherms of samples in set VRnP-*T*.

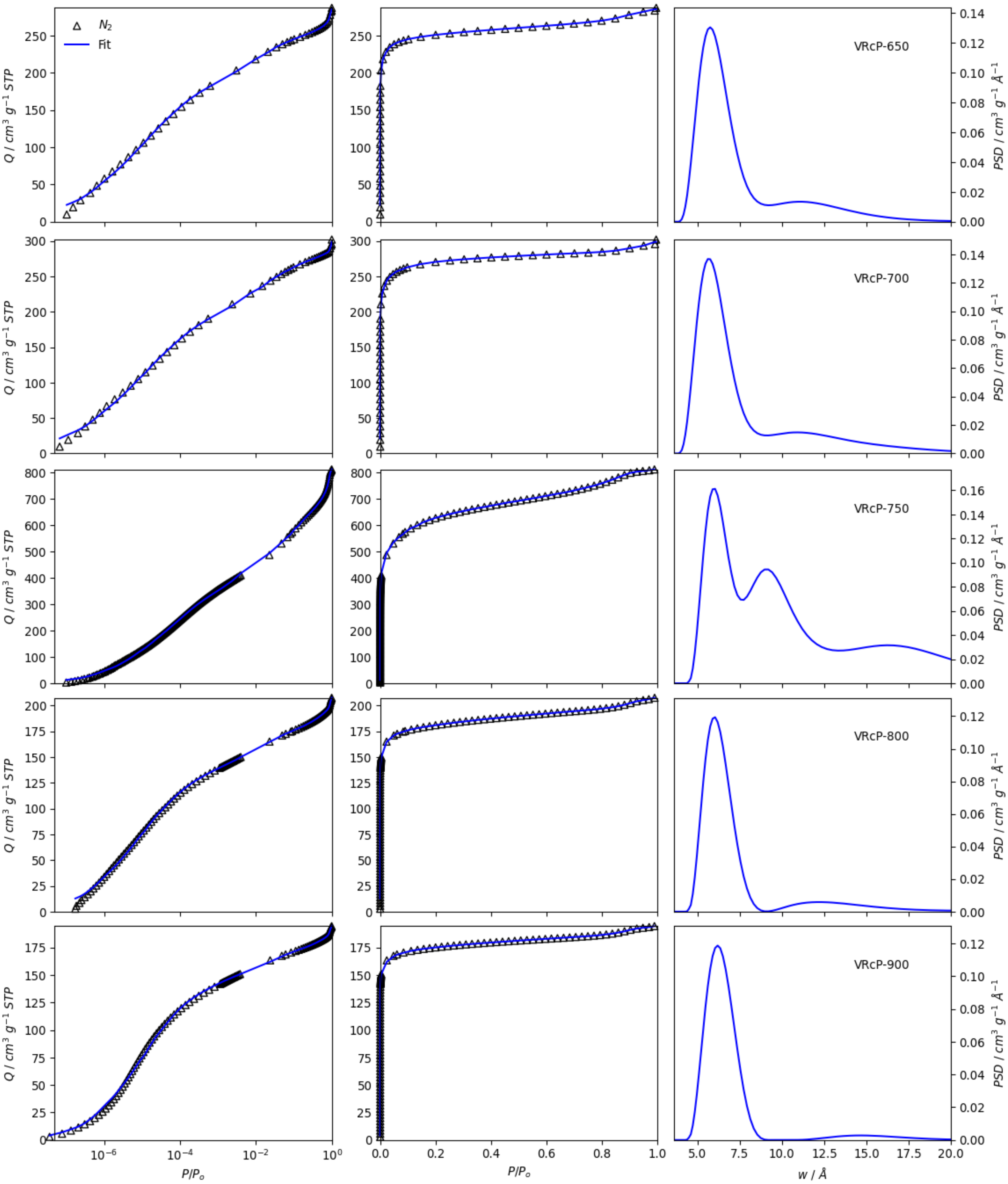

Fig. S31: Fits of N_2 isotherms of samples in set VRcP-*T*.

8. Gas uptake

This section contains comparsion of CO_2 and CH_4 uptakes of the carbons in this work to those in the literature (table S3), as well as all gravimetric uptake isotherms and fits to models (figures S32, S33).

Table S3: Tabulated excess uptake of CO_2 and total uptake of CH_4 at 25 °C and various pressures (bar), of selected samples produced in the work and ACCs in the literature.

Sample	**CO_2 uptake** / mmol g^{-1}			**CH_4 uptake** / mmol g^{-1}			**ref**
	1.0	20	40	1.0	20	35	
VRcP-750	2.9	14.0	16.3	1.3	8.3	10.4	this work
VRnP-750	4.1	12.3	13.3	1.9	8.3	10.0	this work
VRnzZ-50-630	3.5	8.9	9.5	1.2	5.6	6.8	this work
C60-CC-PNP		14.3			7.5		S4
C30-CC-PNP	4.2	11.9			7.0		S4
ACC	2.0			0.7			S5
FIPC	2.8			1.3			S6
FIAC	1.7						S6
Cloth 1		6.0					S7 (commercial)
Cloth 2		7.0					S7 (commercial)
CC-CH	2.5	3.8		1.0	2.3		S8
C60-CCC-PNP		3.3			1.6		S8
C60-CFT-PNP		3.1			1.8		S8

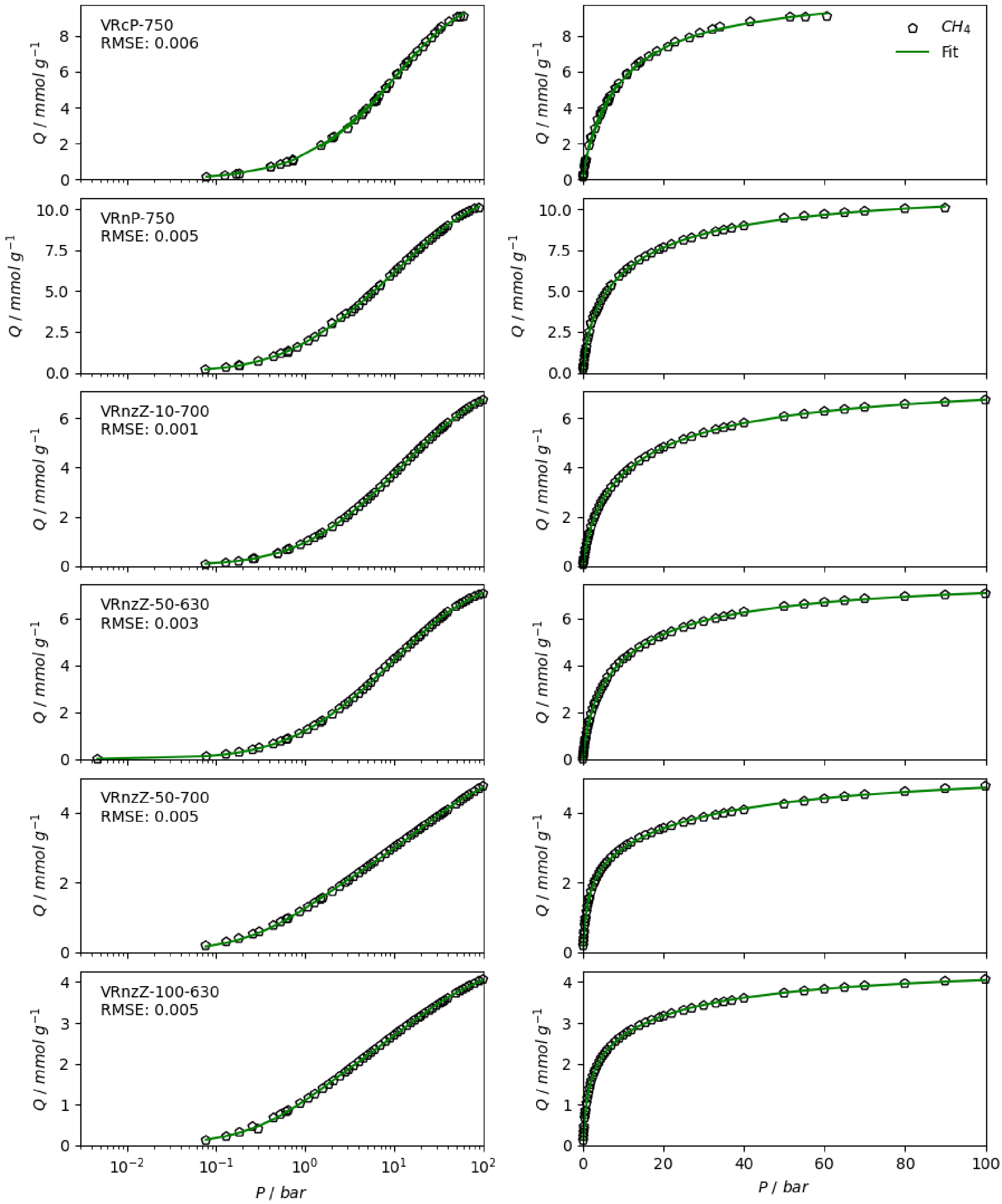

Fig. S32: Excess CH_4 isotherms and fits to double site Langmuir[S9] model for purposes of extracting loadings at specific pressures. Where samples became saturated at some pressure, data after this is excluded for the purposes of the fit.

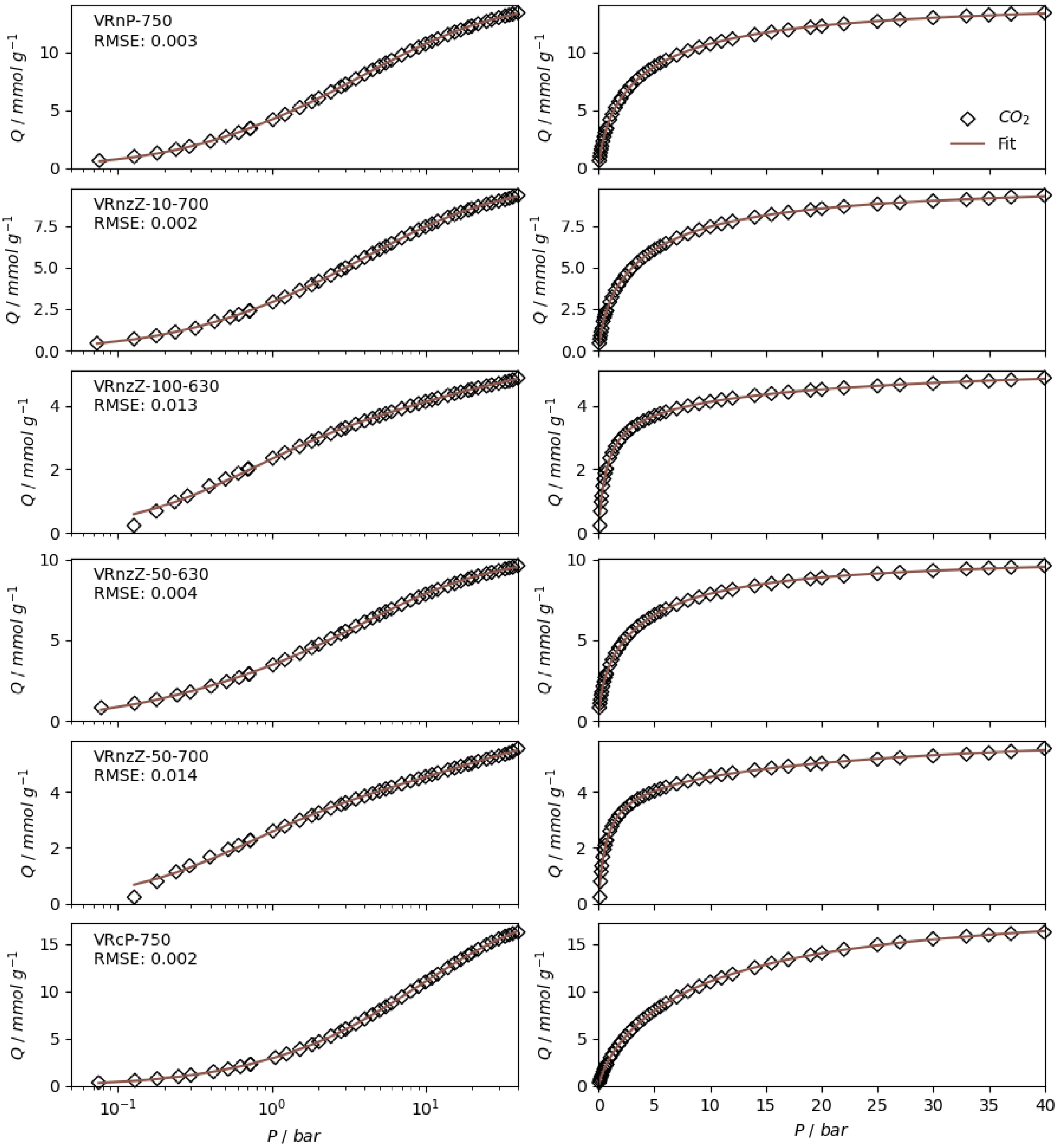

Fig. S33: Excess CO_2 isotherms and fits to double site Langmuir[S9] model for purposes of extracting loadings at specific pressures.

References

(S1) Blankenship, L.S.; Jagiello, J.; and Mokaya, R. "Confirmation of pore formation mechanisms in biochars and activated carbons by dual isotherm analysis." *Materials Advances*, 2022. **3**(9):3961–3971

(S2) Osterrieth, J.W.; Rampersad, J.; Madden, D.; Rampal, N.; Skoric, L.; Connolly, B.; Allendorf, M.D.; Stavila, V.; Snider, J.L.; Ameloot, R.; *et al.* "How reproducible are surface areas calculated from the BET equation?" *Advanced Materials*, 2022. p. 2201502

(S3) Jagiello, J. and Olivier, J.P. "2D-NLDFT adsorption models for carbon slit-shaped pores with surface energetical heterogeneity and geometrical corrugation." *Carbon*, 2013. **55**:70–80

(S4) Attia, N.F.; Jung, M.; Park, J.; Jang, H.; Lee, K.; and Oh, H. "Flexible nanoporous activated carbon cloth for achieving high H2, CH4, and CO2 storage capacities and selective CO2/CH4 separation." *Chemical Engineering Journal*, 2020. **379**:122367

(S5) Kostoglou, N.; Koczwara, C.; Prehal, C.; Terziyska, V.; Babic, B.; Matovic, B.; Constantinides, G.; Tampaxis, C.; Charalambopoulou, G.; Steriotis, T.; Hinder, S.; Baker, M.; Polychronopoulou, K.; Doumanidis, C.; Paris, O.; Mitterer, C.; and Rebholz, C. "Nanoporous activated carbon cloth as a versatile material for hydrogen adsorption, selective gas separation and electrochemical energy storage." *Nano Energy*, 2017. **40**:49–64. doi:10.1016/j.nanoen.2017.07.056

(S6) Rodríguez-Blanco, G.; Giraldo, L.; and Moreno-Piraján, J.C. "Carbon molecular sieves from carbon cloth: Influence of the chemical impregnant on gas separation properties." *Applied Surface Science*, 2010. **256**:5221–5225. doi:10.1016/j.apsusc.2009.12.107

(S7) Lozano-Castello, D.; Monge, J.A.; Lillo, M.; Amoros, D.; and Solano, A. "Advances in the study of methane storage in porous carbonaceous materials." *Fuel*, 2002. **81**(14):1777–803

(S8) Jung, M.; Park, J.; Cho, S.Y.; Elashery, S.E.; Attia, N.F.; and Oh, H. "Flexible carbon sieve based on nanoporous carbon cloth for efficient CO2/CH4 separation." *Surfaces and Interfaces*, 2021. **23**:100960

(S9) Langmuir, I. "The adsorption of gases on plane surfaces of glass, mica and platinum." *Journal of the American Chemical society*, 1918. **40**(9):1361–1403